Supporting Information

Reversible Redox of NADH and NAD^+ at a Hybrid Lipid Bilayer Membrane Using Ubiquinone

Wei Ma,[†] Da-Wei Li,[†] Todd C. Sutherland,[‡] Yang Li,[†] Yi-Tao Long,[*,†] and Hong-Yuan Chen[§]

[†]Shanghai Key Laboratory of Functional Materials Chemistry and Department of Chemistry, East China University of Science and Technology, 130 Meilong Road, Shanghai 200237, P.R. China

[‡]Department of Chemistry, University of Calgary, 2500 University Drive NW, Calgary, Canada T2N1N4

[§]Key Laboratory of Analytical Chemistry for Life Science and Department of Chemistry, Nanjing University, 22 Hankou Road, Nanjing 210093, P.R. China

Table of Contents

S1. Experimental section

Materials. All analytical grade reagents were purchased from Sigma-Aldrich. Egg Phosphatidyl Choline (PC) was from Avanti. NADH and NAD^+ were obtained from Sigma-Aldrich. UHQ II system (Elga) was used to purify water to a resistivity of 18 MΩ • cm for preparation of all solutions. Phosphate buffer solution (PBS) was prepared using Na_2HPO_4 and NaH_2PO_4 and deaerated by purging with nitrogen. Polycarbonate membrane was obtained from Sigma. N_2 (99.998%, prepurified) was obtained from Cryogenic Gases (Detroit, MI). All electrodes for electrochemical experiments were purchased from Shanghai Chenhua Co., Ltd., China. All chemical reagents for synthesis were of analytical grade, obtained from commercial suppliers, and used without further purification unless otherwise noted.

Self-assembled monolayer (SAM) preparation. Immediately before use, the working gold electrode (2 mm diameter) was polished with alumina paste, rinsed with ultrapure water, then rinsed with acetone and dried with N_2. This gold electrode was immersed for 10 min in a hot "piranha" solution ***(3:1 mixture of concentrated H_2SO_4 and 30% H_2O_2; CAUTION: piranha solutions are very aggressive, corrosive solutions, and appropriate safety precautions should be utilized including the use of acid resistant gloves and adequate shielding)***. After copious rinsing with ultrapure water, the gold electrode was electrochemically cleaned by potential cycling in the potential range from -0.30 to 1.50 V *vs* SCE in 0.5 M H_2SO_4 until the typical cyclic voltammogram of clean gold electrode was obtained. After being rinsed with ultrapure water and ethanol and dried with N_2, the gold electrode was immersed in ethanol solution of 1 mM ubiquinone-terminated disulphides (**Q_nS)** or hexanethiol solution (control experiment) over 24 hours. After deposition, **Q_nS**-SAMs were rinsed with copious amounts of ultrapure water and ethanol to remove excess adsorbate and then dried with N_2 to remove residual solvent.

Vesicle preparation.[1-3] Small unilamellar vesicles (SUVs) were prepared by tip sonication. The chloroform solution containing Egg Phosphatidyl Choline (PC) was dried under nitrogen flow until a dry lipid film was formed on the wall of the vial.

This film was further dried in a vacuum-desiccator for 30 min. The dried PC film was then hydrated and resuspended from the walls of the vial in 1 mL of 0.1 M PBS by vigorous vortexing. The cloudy solution was sonicated in a cold bath (<5 °C), 5 times for 3 min each, until the solution became clear. The clear solution was centrifuged at 13000 rpm for 30 min to remove the metal particles. The supernatant was then extruded through a polycarbonate membrane of pore size 100 nm to ensure formation of SUVs. Finally, the vesicle solution was diluted to a concentration of 1.0 $mg \cdot mL^{-1}$. The SUVs solution was then stored at 4 °C for maximum of 2 days. To incorporate $NADH/NAD^+$ into the phospholipid vesicles, $NADH/NAD^+$ was added to the SUVs solution following protein reconstitution methods described elsewhere.[1,4] Typically, 10% $NADH/NAD^+$/lipid (w/w) was used. The re-suspended mixed lipid solutions were used within 2 days. For the control experiments, the vesicles were treated identically to the above procedures except that $NADH/NAD^+$ addition step was omitted.

Formation of supported hybrid lipid bilayer membrane (HBM).[4,5] The fresh $\mathbf{Q_nS}$-SAMs or hexanethiol-SAM (control experiment) were then immediately immersed into the phospholipid vesicles solution to allow self-assembly of ubiquinone-embedded HBM layers ($\mathbf{Q_nS}$-HBMs) or hexanethiol-embedded HBM layers (control experiment).

Electrochemistry. A standard jacketed three-electrode cell was used for electrochemistry. A Pt electrode and saturated calomel electrode (SCE) electrode were used as counter electrode and reference electrode, respectively. For all electrochemical experiments, oxygen was removed by bubbling N_2 through the solution prior to measurements. The temperature was controlled to 25 °C using a circulating water bath through the outer cell jacket. The measurements were performed at CHI 660 electrochemical workstation (Shanghai Chenhua Co., Ltd., China). Impedance measurements were performed using the Zahner electrochemical workstation (Zahner, Germany) with a conventional electrochemical setup. The three-electrode setup consists of a functionalized gold electrode as the working electrode, a Pt counter electrode, and a SCE reference electrode. The impedance

spectra were recorded in the frequency range from 0.1Hz to 100 kHz at the formal potential of the $[Fe(CN)_6]^{3-/4-}$ redox couple. The amplitude of the alternating voltage was 10mV (sinusoidal signal).

X-ray photoelectron spectroscopy (XPS). XPS spectra were obtained on an Axis-165 X-ray photoelectron spectrometer (Kratos Analytical) using a monochromatic Al KR X-ray source (1486.7 eV). Survey spectra (0-1100 eV) were taken at constant analyzer pass energy of 160 eV, and all high-resolution spectra for S_{2p}, N_{1s}, P_{2p}, and Au_{4f} were acquired with a pass energy of 20 eV, a step of 0.1 eV, and a dwell time of 200 ms. The takeoff angle between the film surface and the photoelectron energy analyzer was 90°. The typical operating pressure was around 5 $\times$ 10^{-10} Torr in the analysis chamber. Various scan numbers were carried out for the different elements to obtain the high signal-to-noise ratio. The binding energies were referenced to the $Au_{4f7/2}$ at 84.0 eV, and peaks were fitted using the publicly available XPSPEAK v. 4.1. The Shirley function was used as a background and Gaussian-Lorentzian cross-product was used to fit the individual peaks. The samples for XPS measurements were prepared from the **Q_nS**-SAMs, **Q_nS**-HBMs and **Q_nS**-HBM-NADH/NAD^+ on gold-coated silicon chips (5 mm $\times$ 5 mm size, West Chester, PA U.S.A.). Before the chips were incubated in deaerated solutions, the chips were carefully precleaned by soaking in hot Piranha solution (H_2SO_4/H_2O_2 = 3:1) for 10 min and then sonicated in ultrapure water three times.

Atomic force microscopy (AFM). AFM images were acquired on gold-coated silicon chips (5 mm $\times$ 5 mm size, West Chester, PA U.S.A.) by using Nanoscope IIIa Multimode AFM with an extender electronics module (Veeco, Santa Barbara, CA). Oxide-sharpened silicon nitride cantilevers with a nominal spring constant of $\approx$ 3 N/m were used for experiments. All Imaging was carried out in tapping mode (at oscillation frequencies between 9 and 15 kHz). The scan rates ranged between 1 and 12 Hz.

***In-situ* surface enhanced raman scattering (SERS)**. *In-situ* Raman experiments were made in an optically transparent thin layer electrochemical cell (optical path length is 0.4 ± 0.05 mm) using ubiquinone-embedded HBM immobilized NAD^+ on

gold mesh electrode (**Q_5S**-HBM-NAD^+) as the working electrode, a platinum wire as a counter electrode, and a Ag/AgCl reference electrode via a portable Raman spectrometer (BWS415 i-Raman, BWTEK Inc.). The mesh electrode was aligned such that the laser beam passed through the centre of the working electrode. Potentials were controlled by a CHI1232A electrochemical workstation. For SERS measurements, the spectra were recorded by focusing the 785 nm diode laser (12 mW output power, 10 mW at the sample, 0.02 mm beam diameter) on the surface of the gold mesh electrode with a total accumulation time of 20 s per spectrum. The instrument background was subtracted and baseline corrected with a multiple point linear curve fitting baseline correction. An excitation wavelength of 785 nm was used to induce Raman scattering since it avoids photochemistry and fluorescence background from analytes on electrode, and a Thermo-Electric (TE) cooled detector provides extremely high detection sensitivity. For SERS experiments, the gold mesh electrode was treated by electrochemical roughening procedure, which was used to produce SERS-active rough gold substrates. The procedure consisted of a single cycle in a 1.0 mol/L NaCl solution from -0.50 V to +0.60 V at a rate of 100 $mV \cdot s^{-1}$. Hold times of 30 s at the lower potential and 10 s at the higher potential were used.

Enzymatic assay.[6] A quartz cell containing a **Q_5S**-HBM modified gold mesh electrode (Alfa Aesar, MA, USA, 99.9%, 52 mesh, open area = 62.7%, wire diameter = 0.102 mm), a Pt wire counter electrode and a Ag/AgCl reference electrode via an Ocean Optics DT-minutesi-2 halogen recourse and USB2000+ spectrometer. 120 μL of a 2.4 mM solution of NADH in 50 mM PBS buffer (pH 7.0) was added to PBS in the thin layer quartz cell (optical path length is 0.4 ± 0.05 mm). The mesh electrode was aligned such that the UV-vis beam passed through the centre of the working electrode. Potentials during the UV-vis spectral measurement were controlled by CHI 1232A electrochemical workstation (Shanghai Chenhua Co., Ltd., China). To the above quartz cell, 1 μL of 100 $U \cdot mL^{-1}$ alcohol dehydrogenase (Sigma, Baker's Yeast) and 5 μL of ethanol (Aldrich) were added to the top of the cuvette very slowly to minimize mixing. As the enzyme and ethanol diffused into the beam path the conversion of ethanol to acetaldehyde was assessed by the increase in the NADH

peak at 340 nm. All prepared solutions were deoxygenated for 30 min prior to each experiment and the cell was kept under a nitrogen atmosphere throughout the experiment.

S2. Synthesis and characterization of Q_nS (n=1, 5, 10)

All reactions were monitored by thin layer chromatography (TLC) using silica-coated plates and visualizing under UV light. Light petroleum of the distillation range 60~90 °C was used. Evaporation of solvents was performed at reduced pressure, using a rotary evaporator. THF was distilled from sodium benzophenone ketyl. Column chromatography was performed on silica gel (300~400 mesh). Proton magnetic resonance (^{1}H NMR) spectra were recorded on Bruker FT (500MHz) NMR spectrometers at 25 °C. Proton chemical shifts are expressed in parts per million (ppm, δ scale) and are referenced to residual protons in the NMR solvent ($CHCl_3$, δ 7.26). Data are represented as follows: chemical shift, multiplicity (s = singlet, d = doublet, t = triplet). Carbon nuclear magnetic resonance spectra (^{13}C NMR) were recorded on Bruker FT (126 MHz) NMR spectrometers at 25 °C. Carbon chemical shifts are expressed in parts per million (ppm, δ scale) and are referenced to the carbon resonances of the NMR solvent ($CDCl_3$, δ 77.0). Mass spectra (TOF MS EI$^+$) were recorded under electron impact. The elemental analysis was recorded on the elementar vario EL Ⅲ.

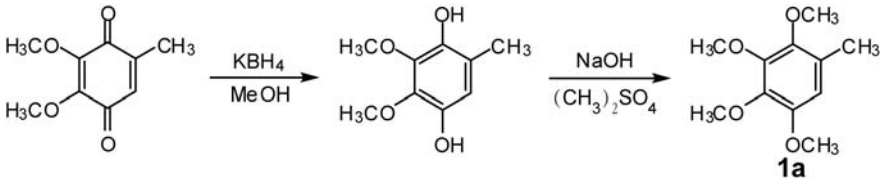

1a

2,3,4,5-tetramethoxytoluene (**1a**). To a solution of 2,3-dimethoxy-5-methyl-l,4-benzoquinone (4.00 g, 21.7 mmol) in methanol (30 ml) at 0 °C was added dropwise, a solution of KBH_4 (5.85 g, 108.5 mmol) in methanol (30 ml).[7] After 30 min, the reaction was quenched by the addition of EtOAc followed by 5% aqueous HCl. The mixture was extracted with EtOAc (3×50 ml) and the organic layer was washed successively with water and brine, dried ($MgSO_4$) and evaporated at reduced pressure. The crude hydroquinone (4.20 g) was dissolved in EtOH (20 ml) and to this solution

at room temperature was added in six portions simultaneously, a solution of NaOH (2.20 g in 6 ml H_2O) and dimethyl sulfate (5.30 ml, 56.0 mmol) at 0 °C. After 45 min, 5% aqueous HCl was added and the mixture was extracted with EtOAc (3×50 ml). The organic layer was washed successively with water and brine, dried ($MgSO_4$) and evaporated to give **1a**[8] (74%) as light yellow liquid. ^{1}H NMR (500.0 MHz): δ 3.99 (s, 12H, 4 × -OCH_3), 2.25 (s, 3H, -CH_3), 6.45(s, H, ArH) ppm.

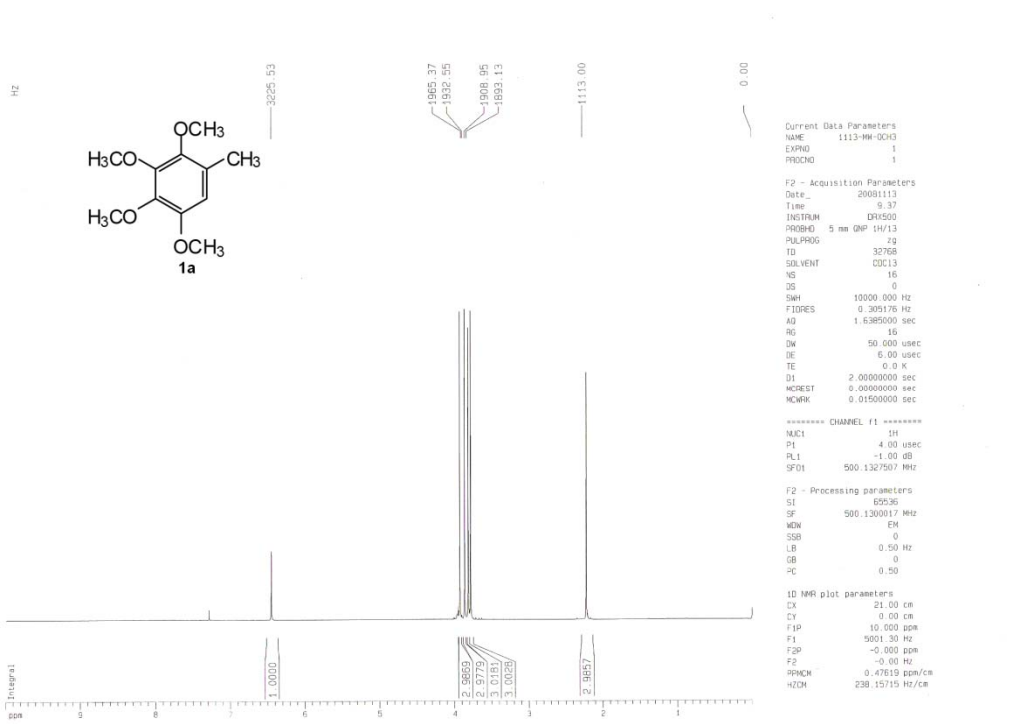

Figure S1. ^{1}H NMR spectrum of **1a** recorded in $CDCl_3$.

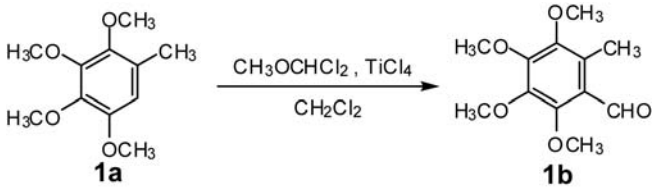

2,3,4,5-tetramethoxy-6-methylbenzaldehyde (**1b**).[9] To a stirred solution of **1a** (4.24 g, 20 mmol) in CH_2Cl_2 (30 ml) was added dichloromethyl methyl ether (6.89 g, 60 mmol) at 0 °C followed by addition of $TiCl_4$ (11.38 g, 60 mmol). The resulting mixture was stirred for 4 h at ambient temperature and then poured into ice water. After stirring vigorously for 10 min, the organic layer was separated. It was washed with water, dried, and evaporated. The residue was chromatographed on silica gel to

give **1b** (90%) as light yellow liquid. ^{1}H NMR (500.0 MHz): δ 3.99~4.02 (s, 12H, 4 × -OCH_3), 2.25 (s, 3H, -CH_3), 10.45 (s, H, -CHO) ppm.

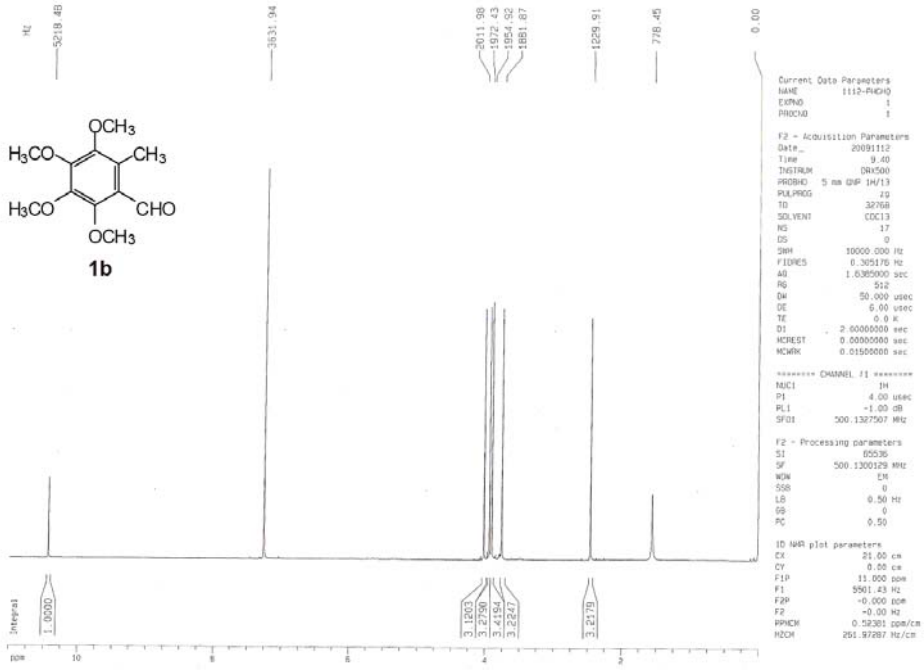

Figure S2. ^{1}H NMR spectrum of **1b** recorded in $CDCl_3$.

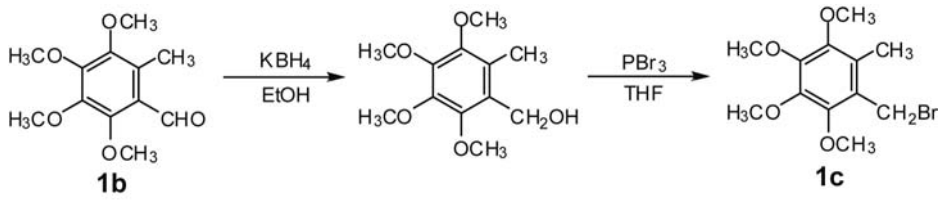

2,3,4,5-tetramethoxy-6-methylbenzyl Bromide (**1c**).[9] To solution of **1b** (1 g, 4.17 mmol) in EtOH (20 ml) was added KBH_4 (0.11 g, 2.06 mmol) at 0 °C. The mixture was stirred for 30 min at the same temperature. The mixture was diluted with brine and the product was extracted with EtOAc. The extract was washed with water, dried, and evaporated to give 2,3,4,5-tetramethoxy-6-methylphenylmethanol. ^{1}H NMR (500.0 MHz): 3.75~3.95 (s, 12H, 4×-OCH_3), 2.25 (s, 3H, -CH_3), 4.65 (s, 2H, -CH_2-), 5.25 (s, H, -OH) ppm. The residue was dissolved in THF (10 ml), PBr_3 (0.44 g, 1.63 mmol) was then added at 0 °C. The resulting mixture was stirred for 30 min and diluted with water. The product was extracted with Et_2O, washed with saturated aqueous $NaHCO_3$, dried, and evaporated. The residue was chromatographed on silica

gel to give **1c** (0.61 g, 61%) as colorless liquid. ^{1}H NMR (500.0 MHz): δ 3.85~4.00 (s, 12H, 4 × -OCH_3), 2.25 (s, 3H, -CH_3), 4.55 (s, 2H, -CH_2Br) ppm.

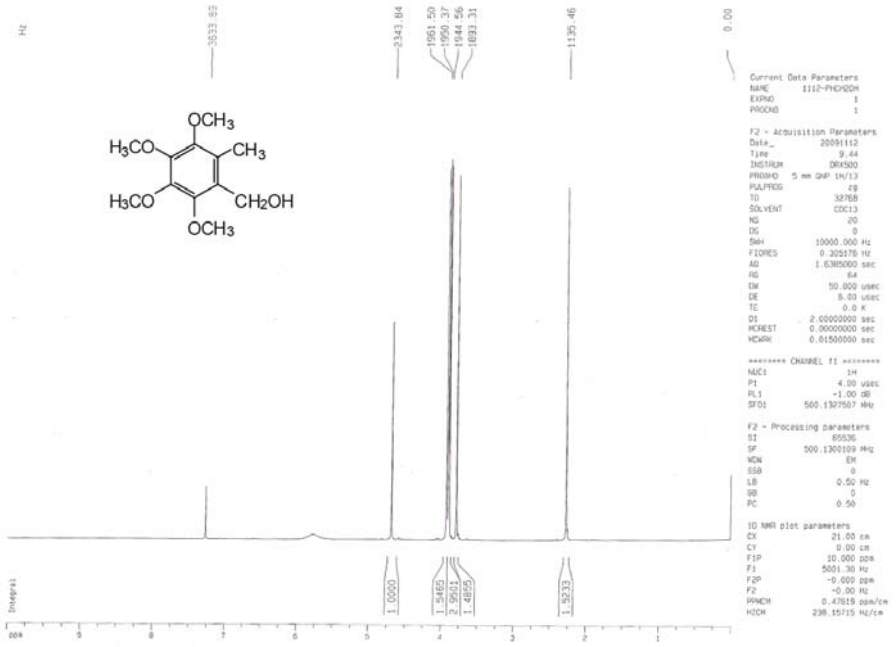

Figure S3. ^{1}H NMR spectrum of 6-hydroxymethylubiquinone recorded in $CDCl_3$.

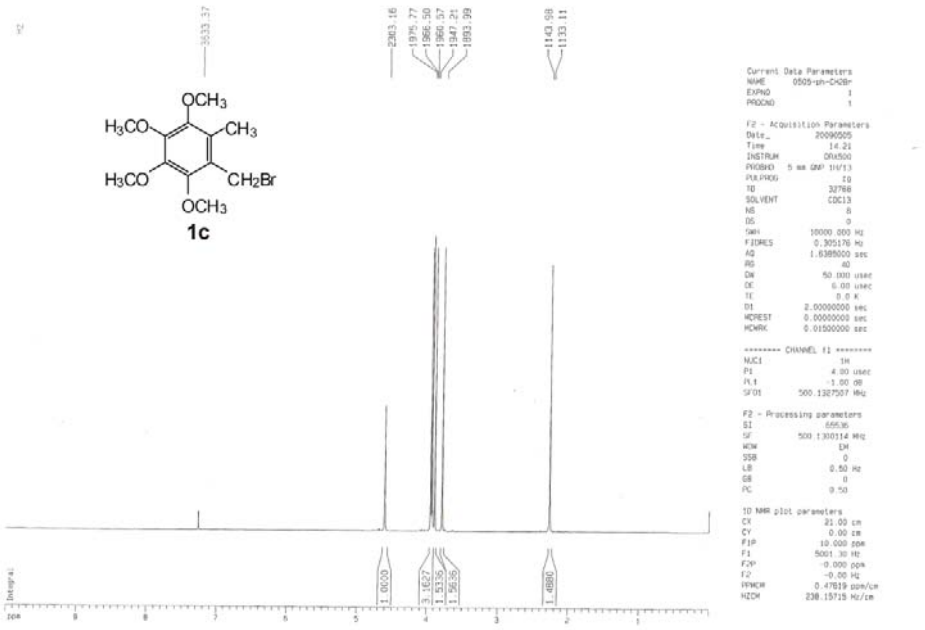

Figure S4. ^{1}H NMR spectrum of **1c** recorded in $CDCl_3$.

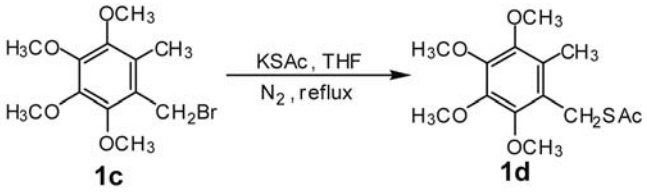

2,3,4,5-tetramethoxy-6-thioacetylmetyl toluene (**1d**).[10] A solution of **1c** (1.2 g, 4.0 mmol) and potassium thioacetate (0.7 g, 6.1 mmol) in dry THF (15 ml) was refluxed for 4 h under the nitrogen atmosphere. The mixture was diluted with brine and the product was extracted with Et_2O and washed with water (50 ml) and dried over $MgSO_4$. After removal of solvent, the residue was purified with column chromatography to give liquid of **1d** (0.65 g, 66%). ^{1}H NMR (500.0 MHz): δ 3.77~3.99 (s, 12H, 4×-OCH_3), 4.22 (s, 2H, -CH_2-), 2.23 (s, 3H, -CH_3), 2.37 (s, 2H, -$COCH_3$) ppm.

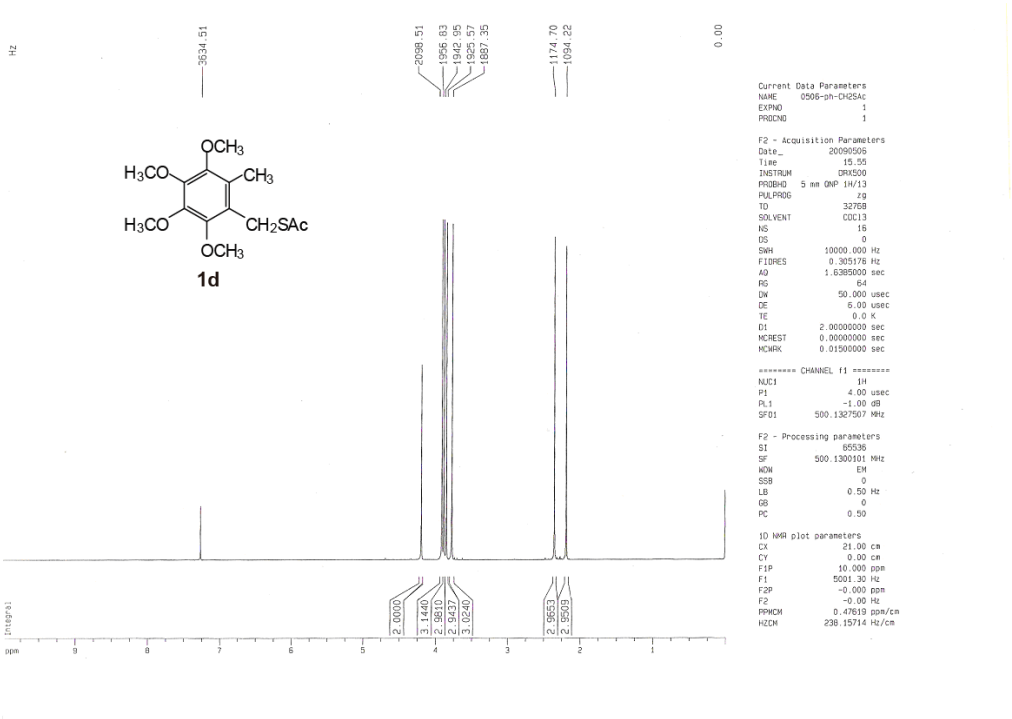

Figure S5. ^{1}H NMR spectrum of **1d** recorded in $CDCl_3$.

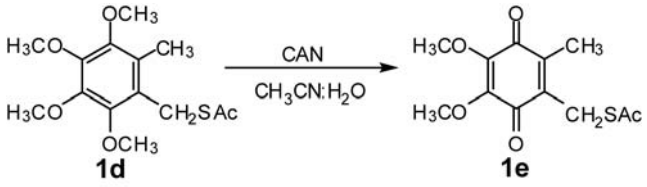

6-thioacetylmetyl ubiquinone (**1e**).[11] To a solution of **1d** (0.24g, 8 mmol) in a 7:4 (v:v) acetonitrile: water mixture (4 ml) was added the solution of cerric ammonium nitrate (CAN) (1.1g, 20 mmol) in a 1:1(v:v) acetonitrile : water mixture (4 ml) at 0 °C over a 20 min period. The resulting solution was stirred at the same temperature for 20 min and room temperature for 10 min before quenching via the addition of water. The resulting reaction mixture was extracted with dichloromethane (10 ml×2) and the combined organic fractions washed with water, dried ($MgSO_4$) and the solvent removed under reduced pressure. The crude product was purified by flash chromatography to provide **1e** (0.18 g, 85%) as an orange oil. ^{1}H NMR (500.0 MHz): δ 4.02 (s, 6H, 2× -OCH_3), 3.97 (s, 2H, -CH_2-S-), 2.18 (s, 3H, -CH_3), 2.37 (s, 2H, -$COCH_3$) ppm.

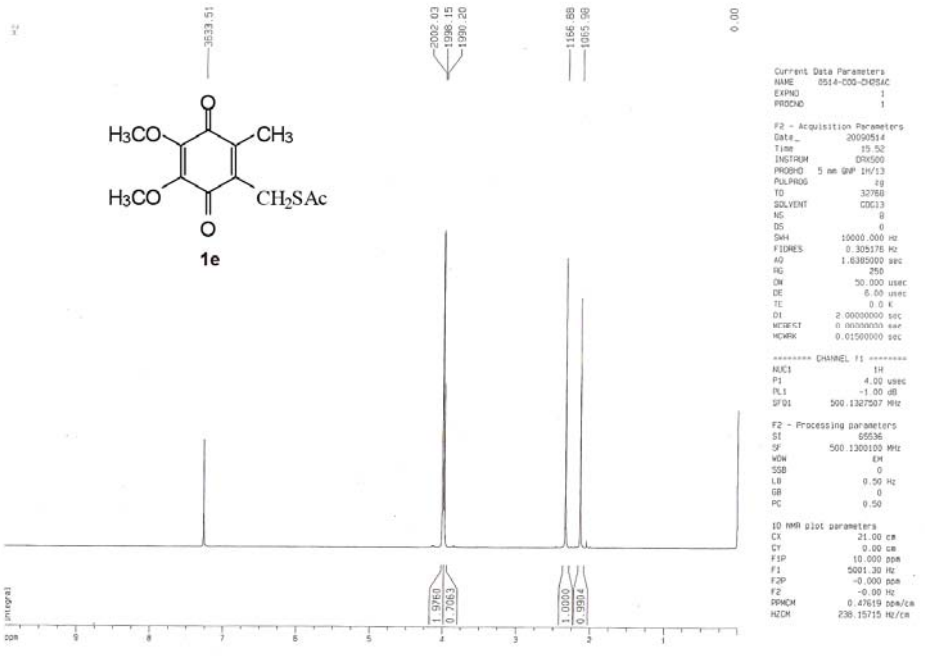

Figure S6. ^{1}H NMR spectrum of **1e** recorded in $CDCl_3$.

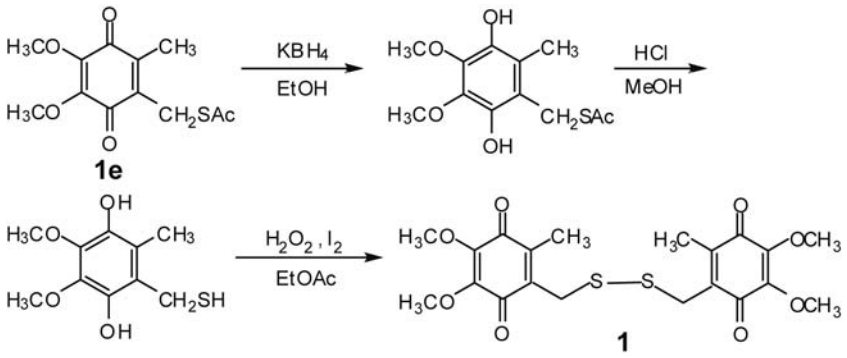

Bis-6-mercapmethyl bisubiquinone (**1**, **Q_1S**). To solution of **1e** (0.27 g, 1.0 mmol) in MeOH (10 ml) was added KBH_4 (0.3 g, 0.5 mmol) at 0 °C under the environment of nitrogen. The mixture was stirred for 30 min at the same temperature. The mixture was diluted with brine and the product was quickly extracted with EtOAc. The extract was evaporated to get 4,5-dimethoxy-2-methy-3-thioacetylmetyl-hydroquinone. The obtained crude product was used in the next reaction without further purification. And then solution of 4,5-dimethoxy-2-methy-3-thioacetylentyl-hydroquinone (1 mmol), methanol (10 ml), and 2 mL of concentrated HCl (35 wt % in water) was heated at 45 °C for 3 h under the protection of nitrogen.[12] The mixture was diluted with water and was extracted with methylene chloride (10 ml ×3). The organic solution was dried over $MgSO_4$. The extract was evaporated to get 6-mercapmetyl hydroubiquinone. The obtained crude product was used in the next reaction without further purification. To a stirred solution of a thiol (1 mmol) in EtOAc (3 ml) was added I_2 (2.5 mg, 0.01 mmol) and 30% H_2O_2 (0.11 ml, 1 mmol) and the mixture was stirred at room temperature for 0.5 h.[13] Saturate aqueous $Na_2S_2O_3$ (15 ml) was added, and the resulting mixture was extracted with EtOAc (15 ml ×3). The combined organic phases were washed with brine (15 ml) and dried ($MgSO_4$). The solvent was evaporated, and the residue was purified by silica gel column chromatography to afford **1** (0.18 g, 42%) as an orange oil. ^{1}H NMR (500.0 MHz): δ 4.02 (s, 12H, 4×-OCH_3), 2.12 (s, 6H, 2×-CH_3), 3.82 (s, 4H, 2×-CH_2); ^{13}C NMR (126 MHz, $CDCl_3$): δ 186.2, 143.2, 61.5, 27.0, 12.5; TOF MS EI+: 454.1, Found: 454.08; Elemental analysis calcd (%) for $C_{20}H_{22}O_8S_2$: C 52.95 , H 4.93; Found: C 52.85, H 4.88.

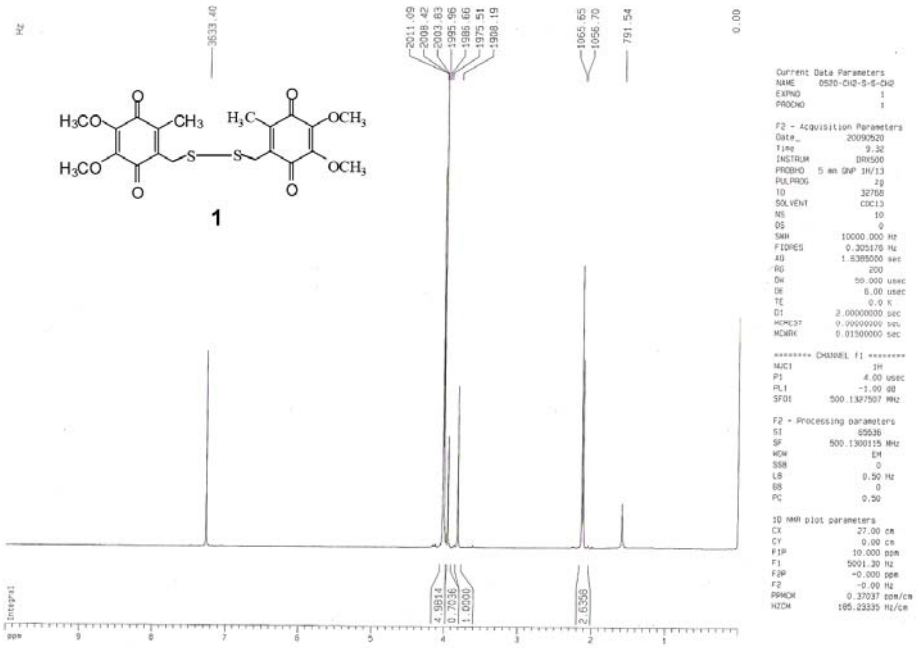

Figure S7. ^{1}H NMR spectrum of **1** recorded in $CDCl_3$.

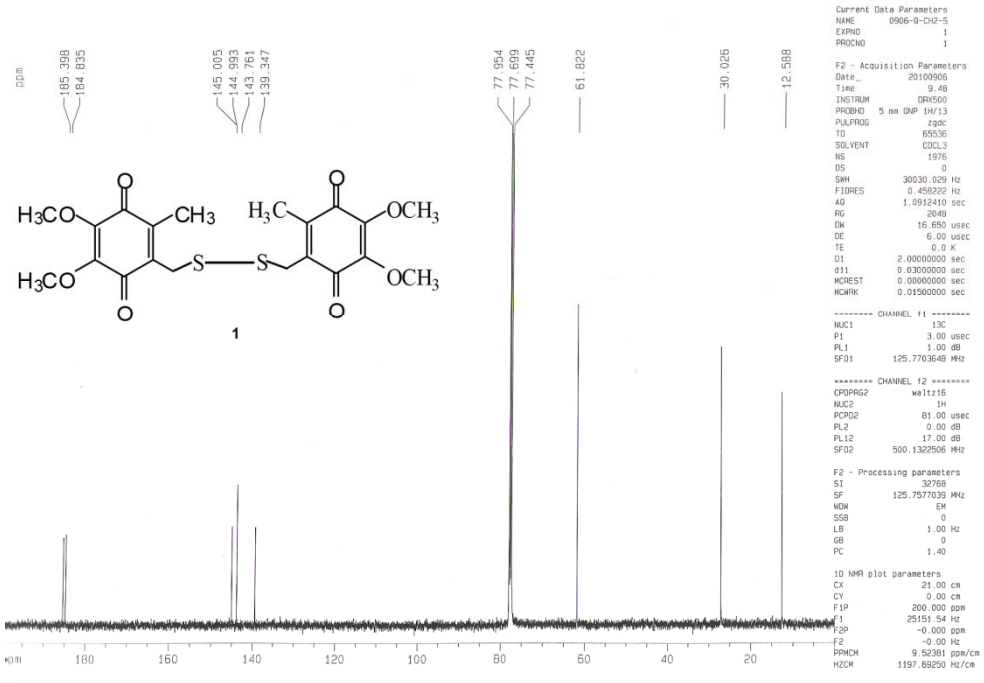

Figure S8. ^{13}C NMR of **1** in $CDCl_3$.

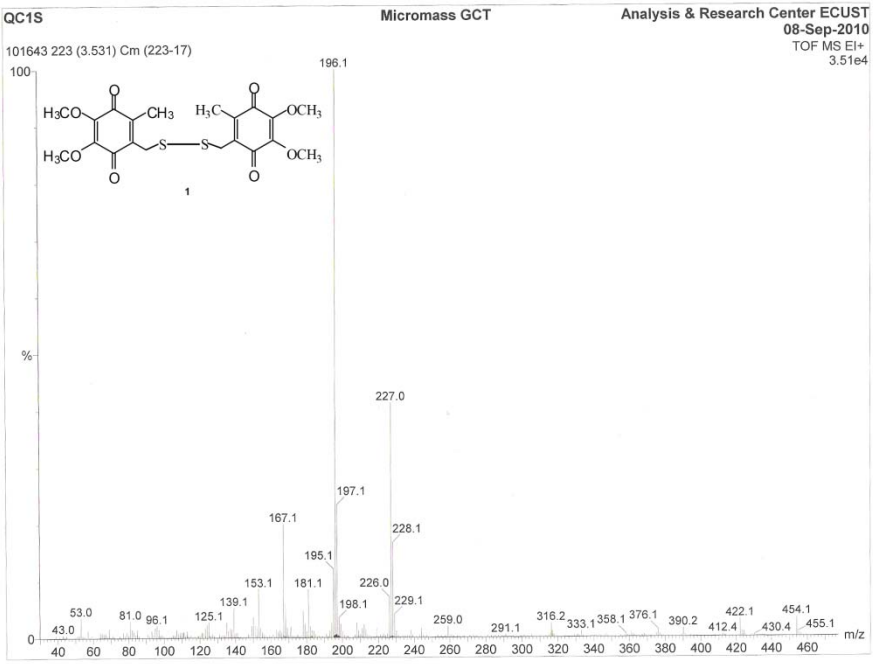

Figure S9. Mass spectum (EI) of **1**.

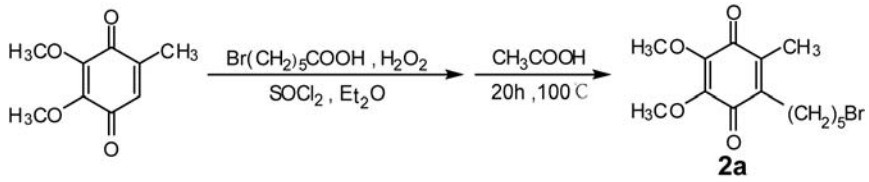

6-(5-Bromopentyl)ubiquinone (**2a**).[14] 6-Bromohexanoic acid (2.94 g, 15.1 mmol) and $SOCl_2$ (1.6 ml, 21.5 mmol) were heated at 90 °C for 15 min. Excess $SOCl_2$ was removed by distillation under reduced pressure and the residue was dissolved in diethyl ether (20 mL) and cooled to 0 °C. Hydrogen peroxide (30%, 1.8 ml) was added, followed by dropwise addition of pyridine (1.4 ml) over 45 min, then diethyl ether (10 ml) was added and after 1 h at room temperature the product was diluted with diethyl ether (150 ml), washed with H_2O (2×70 ml), 1.2 M HCl (70 ml ×2), H_2O (70 ml), 0.5 M $NaHCO_3$ (70 ml ×2), and H_2O (70 ml). After drying over $NaSO_4$ the solvent was removed under reduced pressure, giving white solid 6-Bromohexanoic peroxide as crude, which was used without delay. The crude (2.58 g, 12.5 mmol), 2,3-dimethoxy-5-methyl-1,4-benzoquinone (1.31 g, 7.19 mmol), and acetic acid (60 ml) was synthesized by stirring for 20 h at 100 °C. After cooling to room temperature,

the reaction was diluted with diethyl ether (300 ml), washed with H_2O (3×200 ml), 1 M HCl (250 ml ×3), 0.5 M $NaHCO_3$ (250 ml ×3), and H_2O (200 ml ×3), and dried over $NaSO_4$. Removal of the solvent under reduced pressure gave a reddish solid. The residue was purified by silica gel column chromatography to afford **2a** as a red oil (0.877 g, 37%) . ^{1}H NMR (500 MHz): δ 4.00 (s, 6H, 2×-OCH_3), 3.40 (t, 2H, -CH_2Br), 2.45 (t, 2H, ubiquinone-CH_2-), 2.05 (s, 3H, ubiquinone -CH_3), 1.80(s, 2H, -CH_2-CH_2Br), 1.40~1.55 (m, 4H, -$(CH_2)_2$-) ppm;

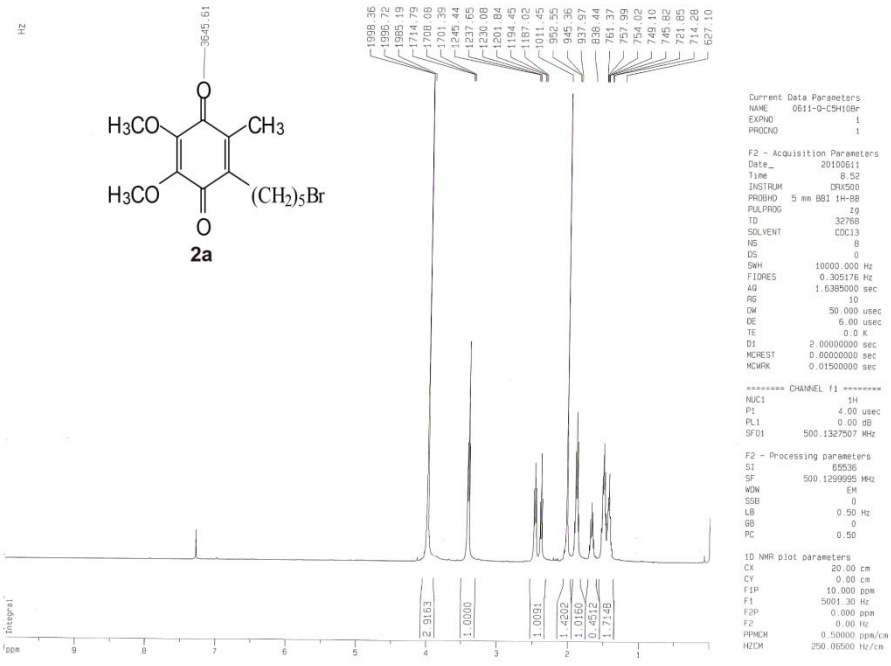

Figure S10. ^{1}H NMR of **2a** in $CDCl_3$.

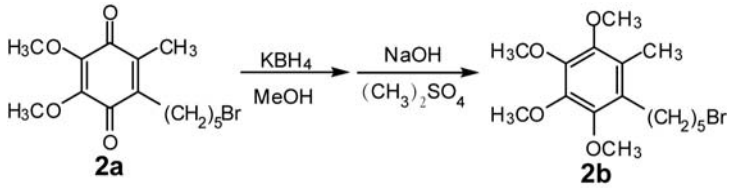

2,3,4,5-tetramethoxy-6-(5-Bromopentyl)-toluene (**2b**). Synthetic step of **2b** is similar to afford **1a**. ^{1}H NMR (500 MHz): δ 3.90 (s, 6H, 2×-OCH_3), 3.75 (s, 6H, 2×-OCH_3), 3.35 (t, 2H, -CH_2Br), 2.55 (t, 2H, ubiquinone-CH_2-), 2.05(s, 3H, ubiquinone -CH_3), 1.82(s, 2H,-CH_2-CH_2Br), 1.35~1.52 (m, 4H, -$(CH_2)_2$-) ppm.

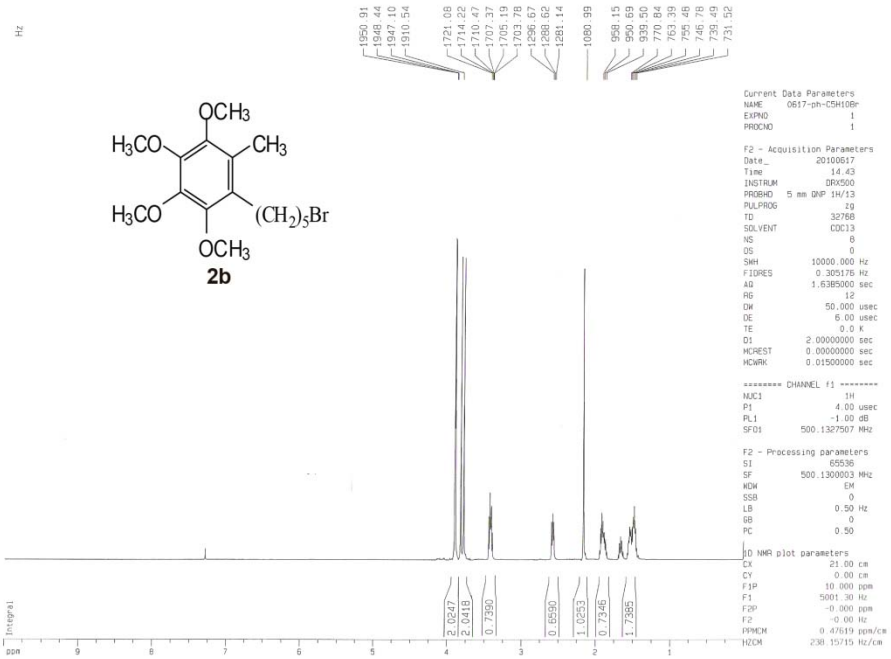

Figure S11. ^{1}H NMR of **2b** in $CDCl_3$.

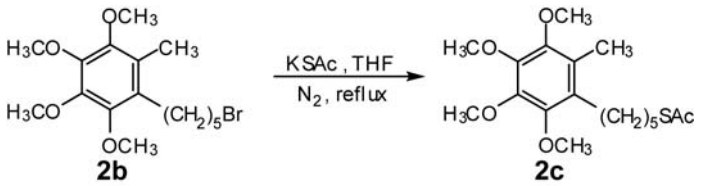

2,3,4,5-tetramethoxy-6-(5-thioacetylpentyl)-toluene (**2c**). Synthetic step of **2c** is similar to afford **1d**. ^{1}H NMR (500 MHz): δ 3.80~3.95 (s, 12H, 4×-OCH_3), 2.82 (t, 2H, -CH_2S-), 2.44(t, 2H, ubiquinone-CH_2-), 2.26(t, 3H, -$COCH_3$), 1.97 (s, 3H, ubiquinone-CH_3), 1.57 (t, 2H, -CH_2CH_2S-), 1.21~1.44 (m, 4H, -$(CH_2)_2$-) ppm.

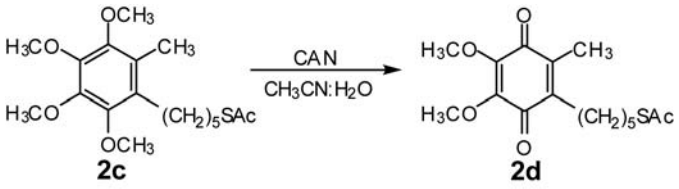

6-(5-thioacetylpentyl)-ubiquinone (**2d**). Synthetic step of **2d** is similar to afford **1e**. ^{1}H NMR (500 MHz): δ 3.92 (s, 6H, 2×-OCH_3), 2.78 (t, 2H, -CH_2S-), 2.40(t, 2H, ubiquinone-CH_2-), 2.23(t, 3H, -$COCH_3$), 1.90 (s, 3H, ubiquinone-CH_3), 1.52 (t, 2H, -CH_2CH_2S-), 1.23~1.42 (m, 4H, -$(CH_2)_2$-) ppm.

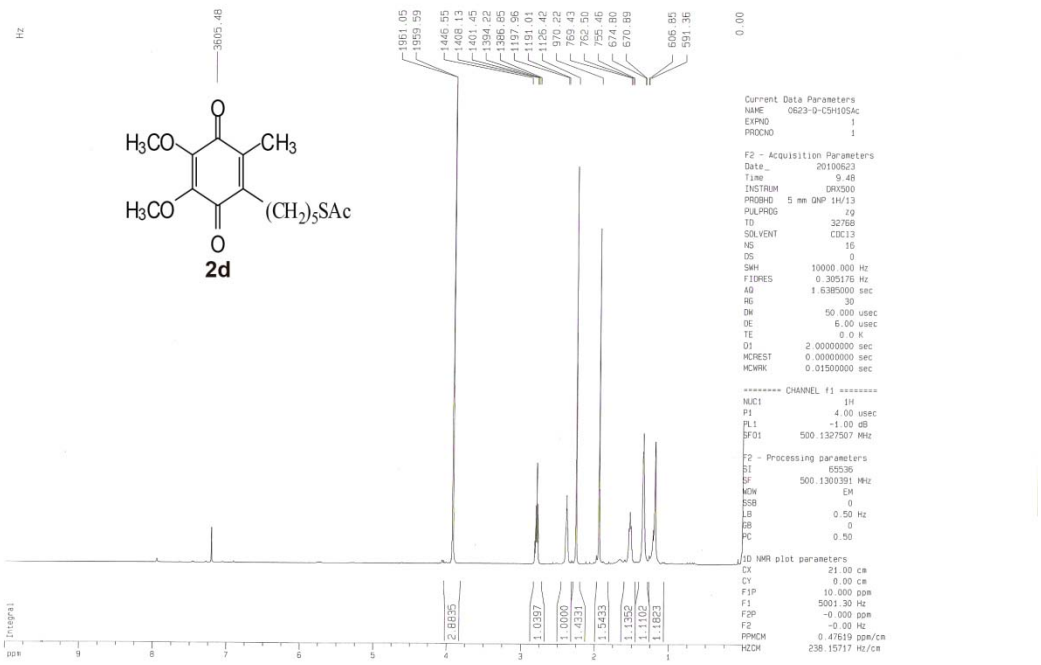

Figure S12. ^{1}H NMR of **2d** in $CDCl_3$.

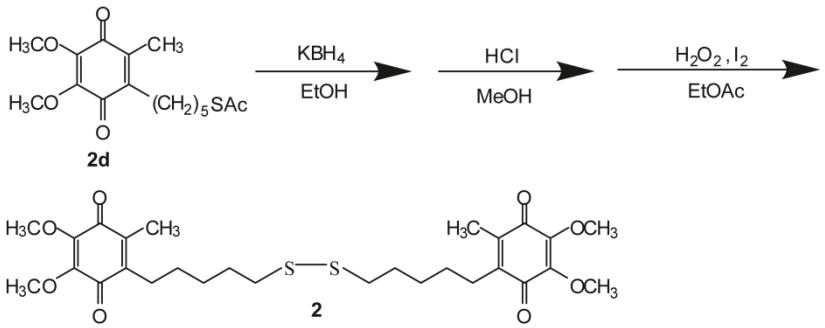

Bis-6-(10-Mercaptopentyl)-bisubiquinone (**2**, **Q_5S**). Synthetic step of **2** is similar to afford **1**. ^{1}H NMR (500 MHz): δ 3.95 (s, 6H, 2×-OCH_3), 2.40 (t, 2H, ubiquinone-CH_2-), 2.06 (s, 3H, ubiquinone-CH_3), 2.55 (t, 2H, -CH_2S-), 1.72 (t, 2H, -CH_2CH_2S-), 1.35~1.47 (m, 4H, -$(CH_2)_2$-) ppm; ^{13}C NMR (126 MHz, CDCl3): δ 186.2, 143.2, 61.5, 39.0, 28.5, 13.0; TOF MS EI+: 454.1, Found: 454.08; TOF MS EI^+: 566.2/567.2, Found: 566.2/567.2; Elemental analysis calcd (%) for $C_{28}H_{38}O_8S_2$: C 59.34, H 6.76; Found: C 59.33, H 6.74.

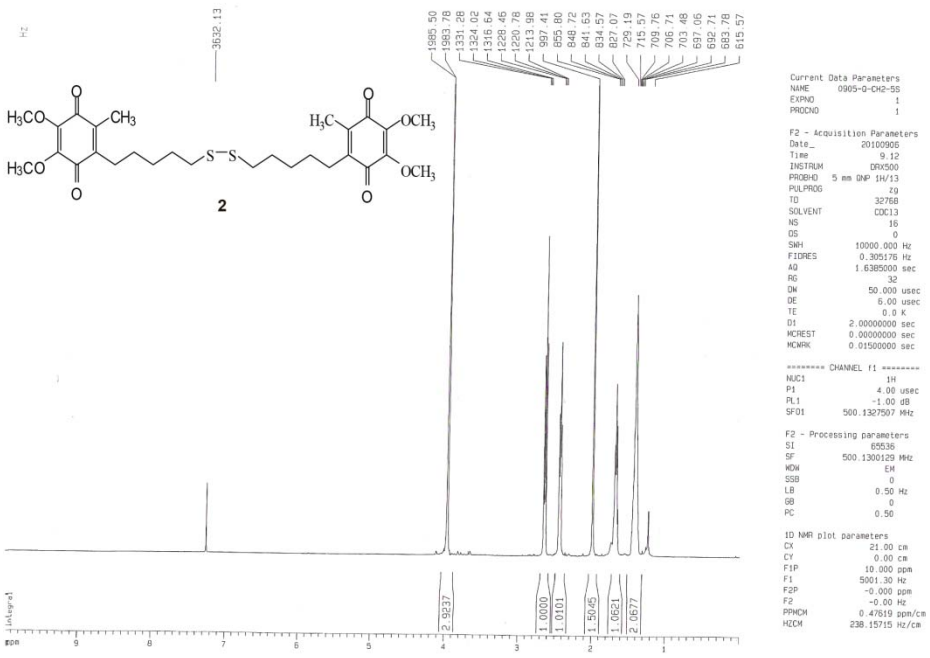

Figure S13. ^{1}H NMR of **2** in $CDCl_3$.

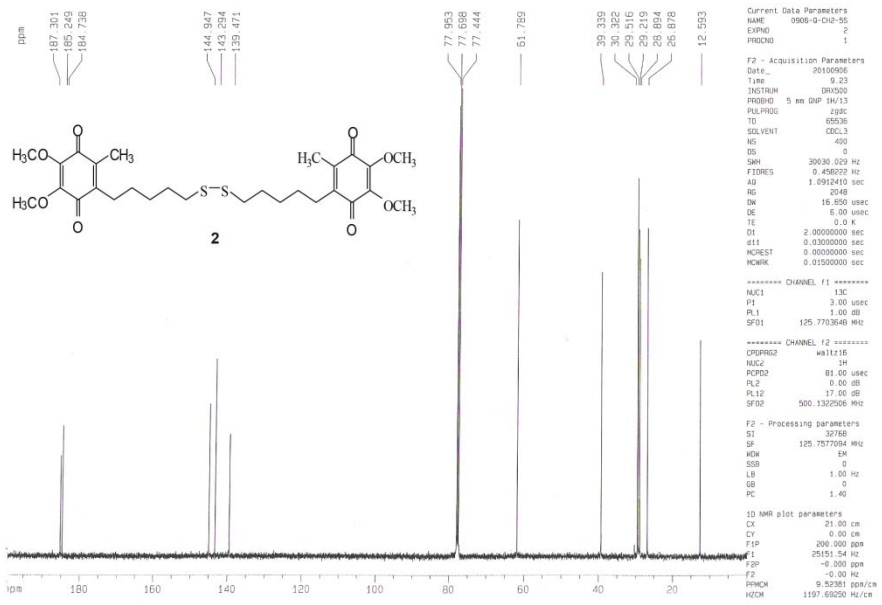

Figure S14. ^{13}C NMR of **2** in $CDCl_3$.

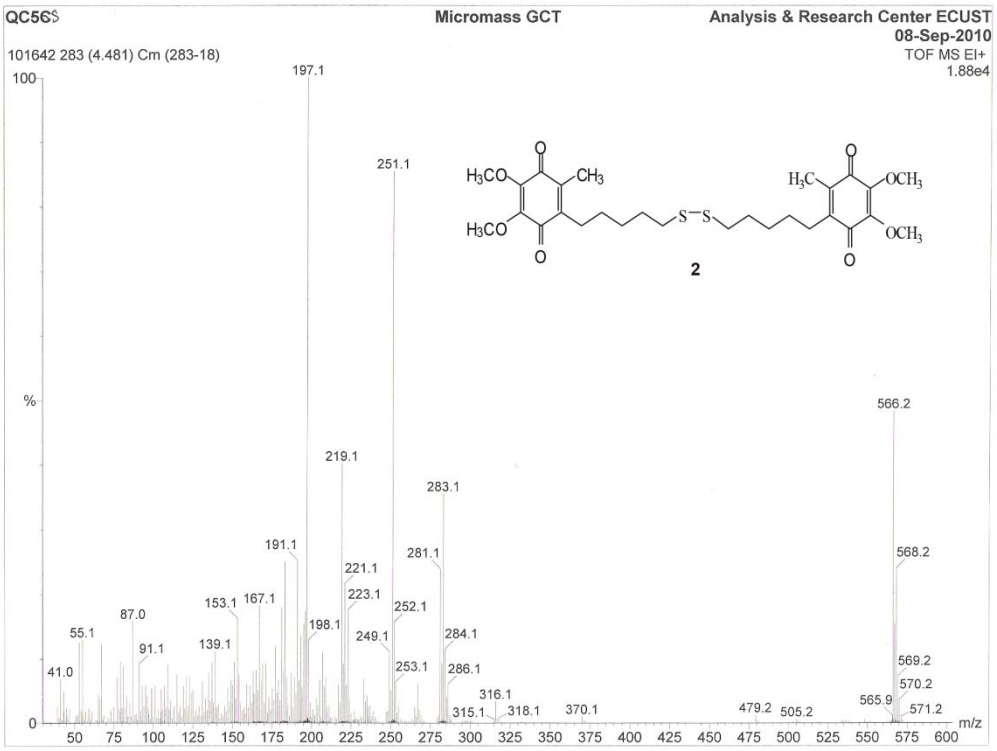

Figure S15. Mass spectum (EI) of **2**.

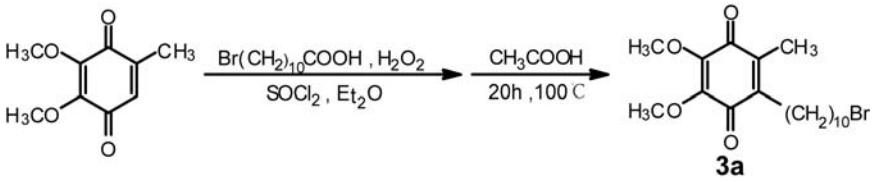

6-(10-Bromodecyl)-ubiquinone (**3a**).[14] 11-bromoundecanoic acid (4.00 g, 15.1 mmol) and $SOCl_2$ (1.6 ml, 21.5 mmol) were heated at 90 °C for 15 min (25). Excess $SOCl_2$ was removed by distillation under reduced pressure and the residue was dissolved in diethyl ether (20 mL) and cooled to 0 °C. Hydrogen peroxide (30%, 1.8 ml) was added, followed by dropwise addition of pyridine (1.4 ml) over 45 min, then diethyl ether (10 ml) was added and after 1 h at room temperature the product was diluted with diethyl ether (150 ml), washed with H_2O (2×70 ml), 1.2 M HCl (70 ml ×2), H_2O (70 ml), 0.5 M $NaHCO_3$ (70 ml ×2), and H_2O (70 ml). After drying over $NaSO_4$ the solvent was removed under reduced pressure, giving white solid 11-bromoundecanoic peroxide as crude, which was used without delay. The crude (3.51 g, 12.5 mmol), 2,3-dimethoxy-5-methyl-1,4-benzoquinone (1.31 g, 7.19 mmol), and acetic acid (60 ml) was synthesized by stirring for 20 h at 100 °C. After cooling to room temperature,

the reaction was diluted with diethyl ether (300 ml), washed with H_2O (3×200 ml), 1 M HCl (250 ml ×3), 0.5 M $NaHCO_3$ (250 ml ×3), and H_2O (200 ml ×3), and dried over $NaSO_4$. Removal of the solvent under reduced pressure gave a reddish solid. The residue was purified by silica gel column chromatography to afford **3a** as a red oil (1.07 g, 37%).δ ^{1}H NMR (500 MHz): 4.00 (s, 6H, 2×-OCH_3), 3.43 (t, 2H, -CH_2Br), 2.45 (t, 2H, ubiquinone-CH_2-), 2.05 (s, 3H, ubiquinone -CH_3), 1.87(s, 2H, -CH_2-CH_2Br), 1.25~1.47 (m, 14H, -$(CH_2)_7$-) ppm; TOF MS EI$^+$: 400.2/402.2; found 400.12/402.12.

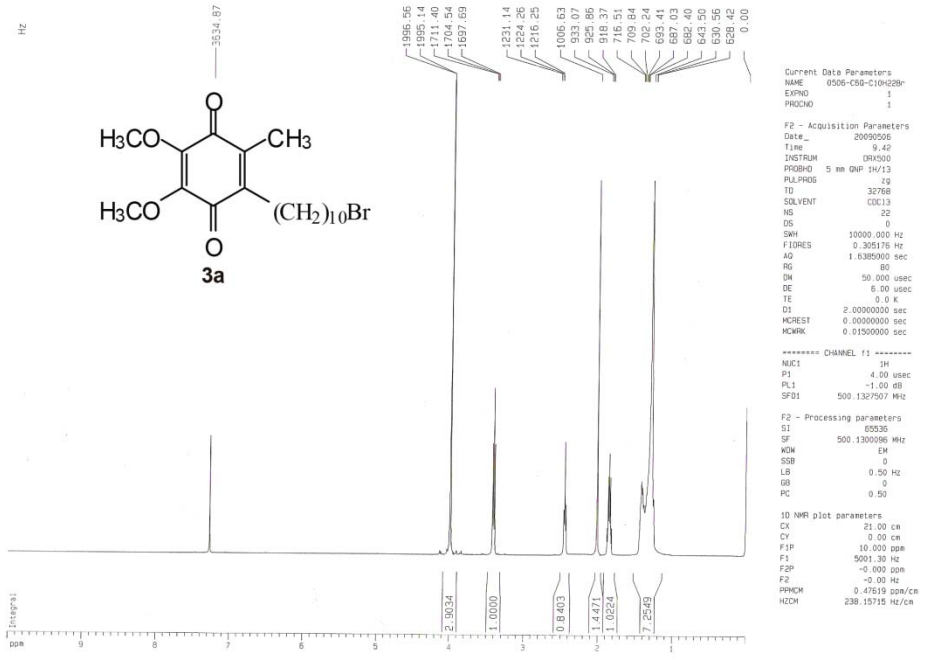

Figure S16. ^{1}H NMR of **3a** in $CDCl_3$.

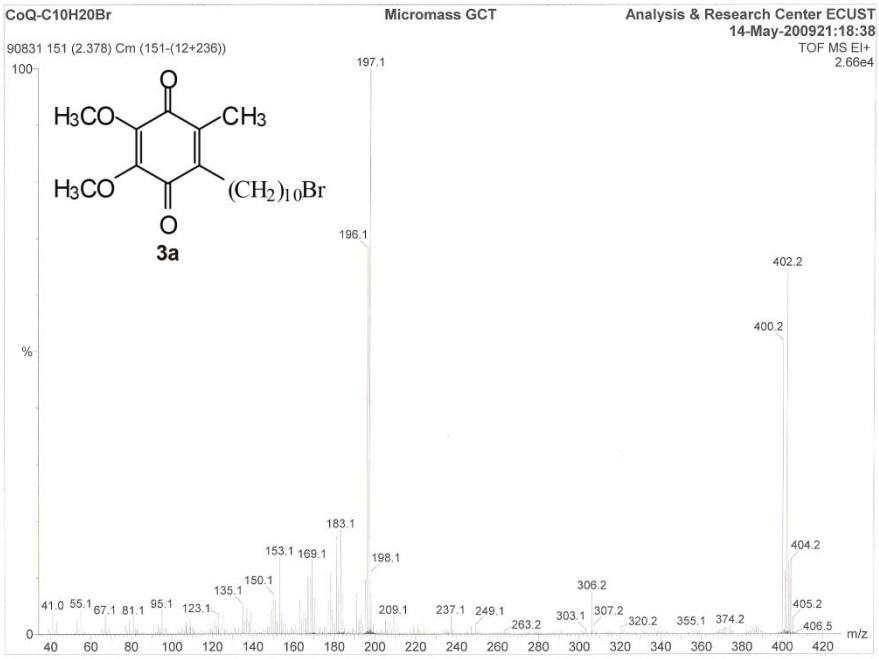

Figure S17. Mass spectum (EI) of **3a**.

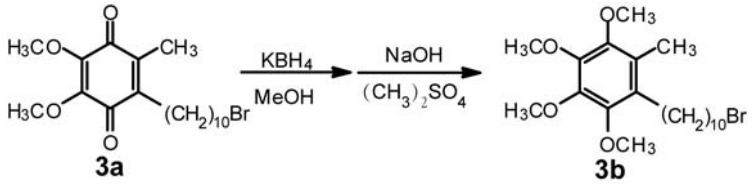

2,3,4,5-tetramethoxy-6-(10-Bromodecyl)-toluene (**3b**). Synthetic step of **3b** is similar to afford **1a**. ^{1}H NMR (500 MHz): δ 4.00 (s, 12H, 4×-OCH_3), 3.43 (t, 2H, -CH_2Br), 2.45 (t, 2H, ubiquinone-CH_2-), 2.05(s, 3H, ubiquinone -CH_3), 1.87(s, 2H,-CH_2-CH_2Br), 1.25~1.47 (m, 14H, -$(CH_2)_7$-) ppm.

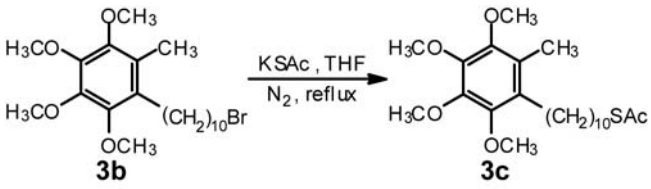

2,3,4,5-tetramethoxy-6-(10-thioacetyldecyl)-toluene (**3c**). Synthetic step of **3c** is similar to afford **1d**. ^{1}H NMR (500 MHz): δ 3.80~3.95 (s, 12H, 4×-OCH_3), 2.55 (t, 2H, ubiquinone-CH_2-), 2.17(s, 3H, -CH_3), 2.32 (s, 3H, -$COCH_3$) , 2.87 (t, 2H, -CH_2S-), 1.62 (t, 2H, -CH_2CH_2S-), 1.25~1.47 (m, 14H, -$(CH_2)_7$-) ppm.

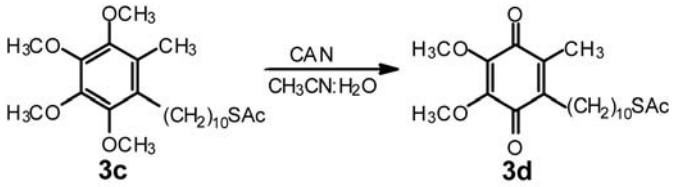

6-(10-thioacetyldecyl)-ubiquinone (**3d**). Synthetic step of **3d** is similar to afford **1e**. ^{1}H NMR (500 MHz): δ 4.00 (s, 6H, 2×-OCH_3), 2.88 (t, 2H, -CH_2S-), 2.45(t, 2H, ubiquinone-CH_2-), 2.36(t, 3H, -$COCH_3$), 2.00 (s, 3H, ubiquinone-CH_3), 1.57 (t, 2H, -CH_2CH_2S-), 1.23~1.42 (m, 14H, -$(CH_2)_7$-) ppm.

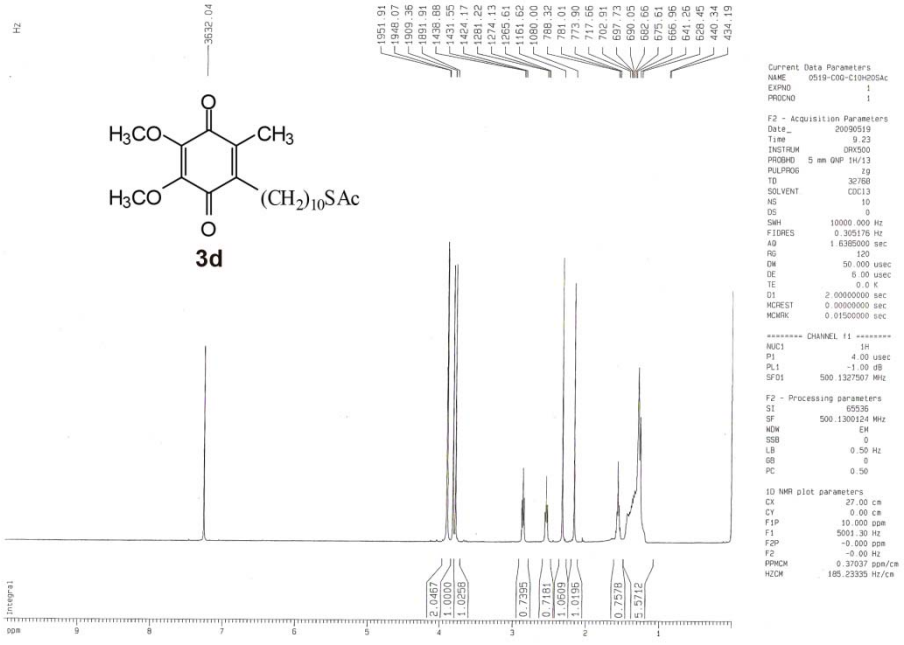

Figure S18. ^{1}H NMR of **3d** in $CDCl_3$.

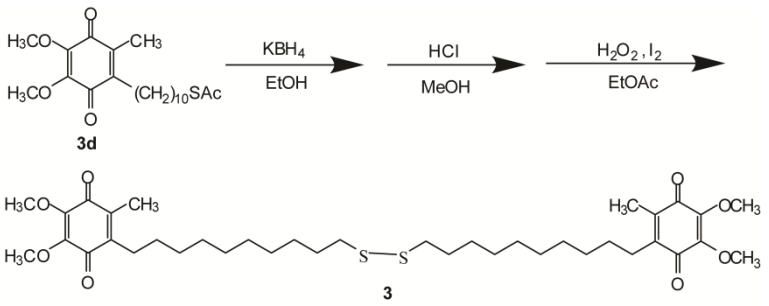

Bis-6-(10-Mercaptodecyl)-bisubiquinone (**3**, **$Q_{10}S$**). Synthetic step of **3** is similar to afford **1**. ^{1}H NMR (500 MHz): 3.98 (s, 6H, 2×-OCH_3), 2.45 (t, 2H, ubiquinone-CH_2-), 2.06 (s, 3H, ubiquinone-CH_3), 2.67 (t, 2H, -CH_2S-), 1.67 (t, 2H, -CH_2CH_2S-), 1.25~1.42 (m, 14H, -$(CH_2)_7$-) ppm; ^{13}C NMR (126 MHz, $CDCl_3$): δ 186.2, 142.5, 61.8, 39.2, 29.3, 12.5; TOF MS EI^+: 706.4/708.4, Found: 706.36/707.36. Elemental analysis calcd (%) for $C_{38}H_{58}O_8S_2$: C 64.56, H 8.27; Found: C 64.64, H 8.21.

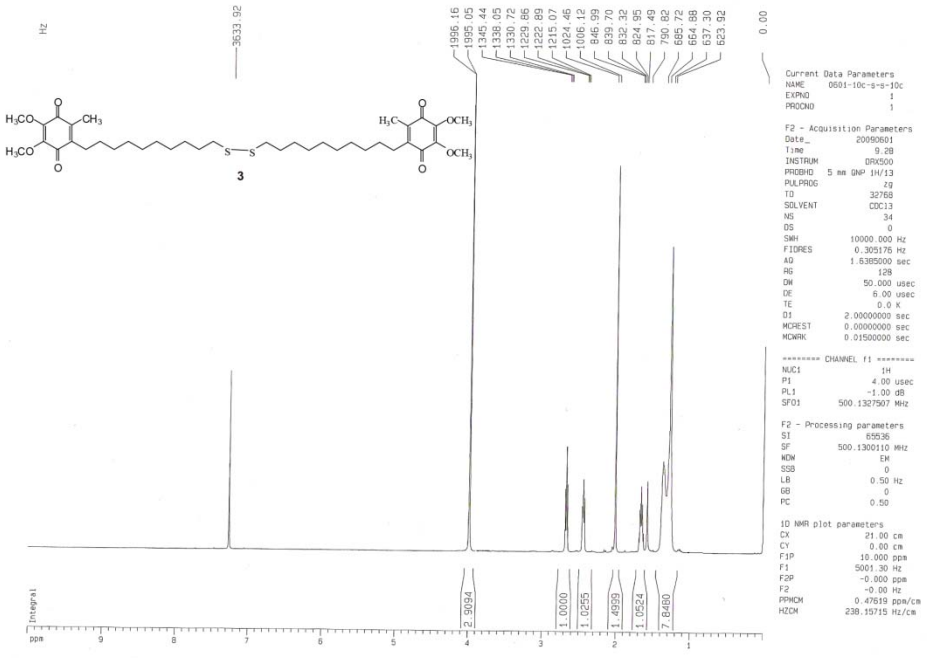

Figure S19. ^{1}H NMR of **3** in $CDCl_3$.

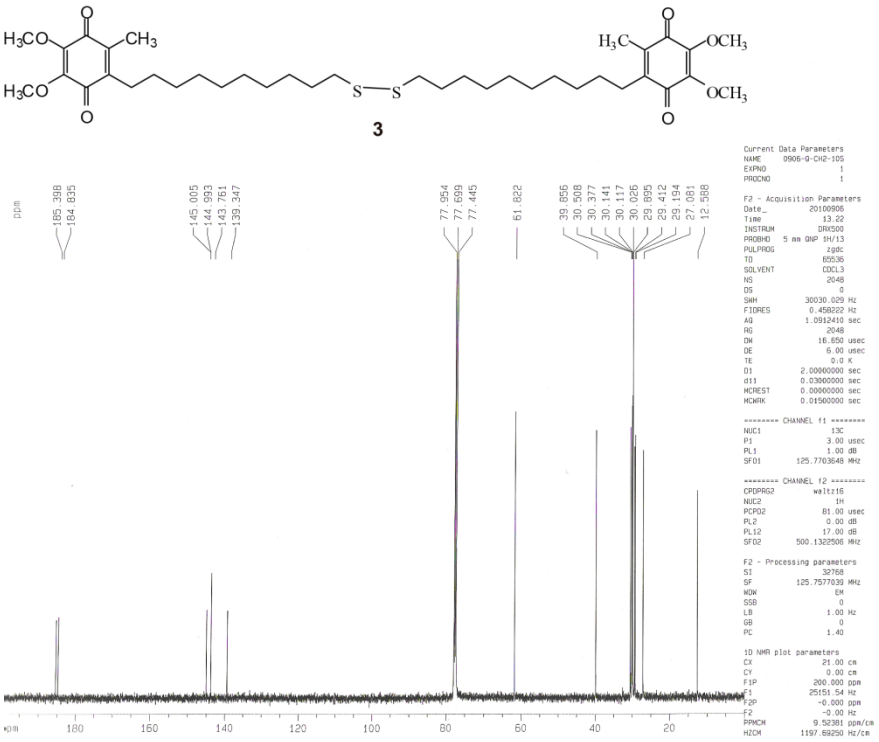

Figure S20. ^{13}C NMR of **3** in $CDCl_3$.

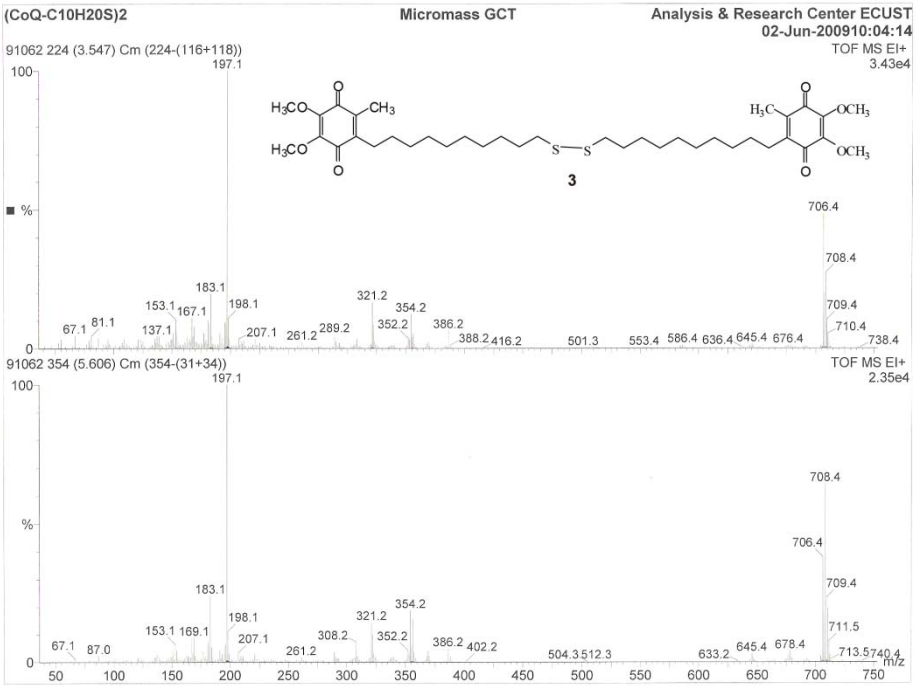

Figure S21. Mass spectum (EI) of **3**.

S3. Electrochemical impedance spectroscopy (EIS)

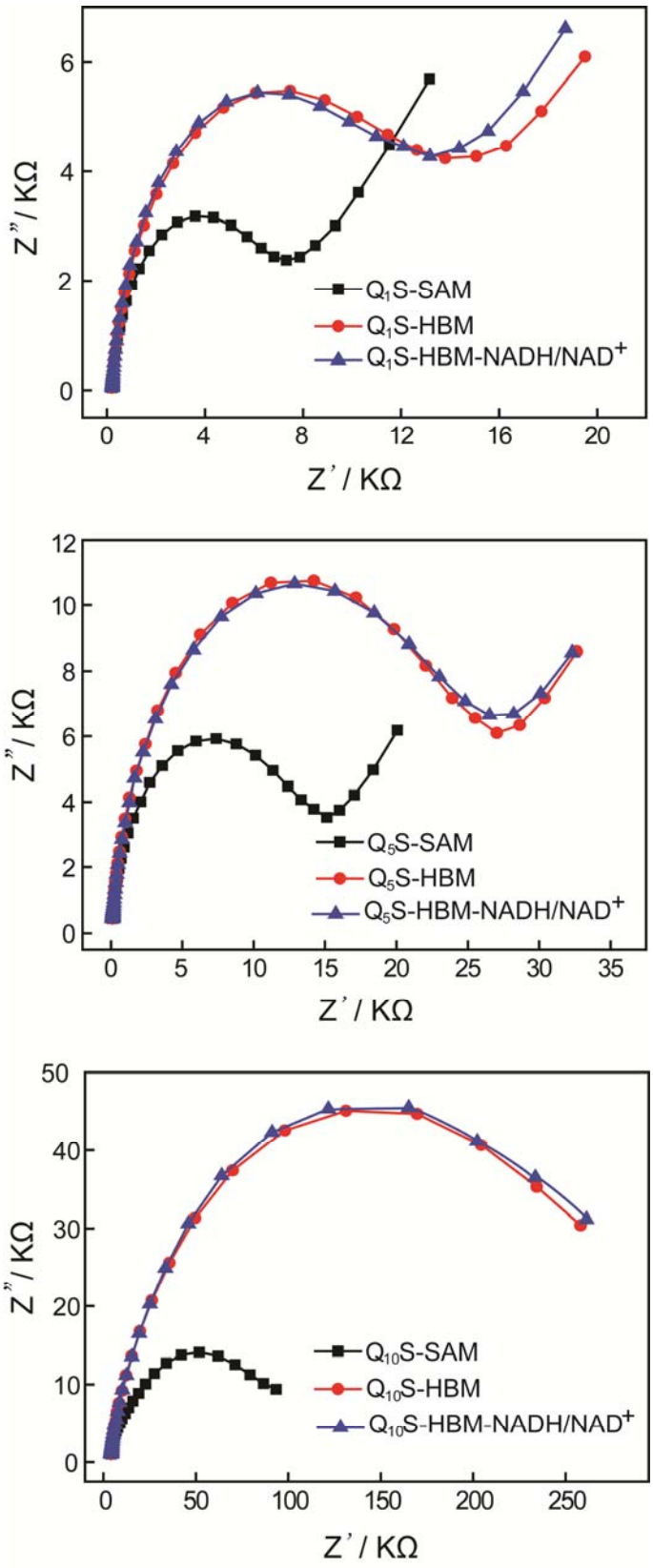

Figure S22. Nyquist plot for the Faradaic impedance before and after formation of HBM (with and without $NADH/NAD^+$) measured on a ubiquinone functionalized

gold electrode. The spectra were recorded in PBS containing 1 mM $[Fe(CN)6]^{3-/4-}$ as a redox probe, using a frequency range from 100 kHz to 0.1Hz with 10 mV excitation signal. The ESI was measured at midpoint potential of $[Fe(CN)6]^{3-/4-}$ vs SCE. The measured potentials were 0.220 V vs SCE, 0.214 V vs SCE, and 0.210 V vs SCE for **Q_1S**-SAM, **Q_1S**-HBM, and **Q_1S**-HBM-NADH/NAD^+, respectively; The measured potential were 0.225 V vs SCE, 0.234 V vs SCE, and 0.236 V vs SCE for **Q_5S**-SAM, **Q_5S**-HBM, and **Q_5S**-HBM-NADH/NAD^+, respectively; The measured potential were 0.220 V vs SCE, 0.244 V vs SCE, and 0.240 V vs SCE for **Q_{10}S**-SAM, **Q_{10}S**-HBM, and **Q_{10}S**-HBM-NADH/NAD^+, respectively.

Hybrid lipid bilayers were characterized with electrochemical impedance spectroscopy (EIS). Figure S22 shows the EIS results in the form of Nyquist plots, in which the diameter of the halfcircle increased significantly when the **Q_nS**-SAMs is embedded in HBM systems. The diameter of the Nyquist halfcircle is equivalent with and without NADH/NAD^+. It is immediately clear that inclusion of NADH/NAD^+ has negligible effect on the double layer capacitance of the hybrid membrane. This indicates that NADH/NAD^+ does not induce large defects in the hybrid bilayer.

S4. High-resolution X-ray photoelectron spectroscopy (XPS)

The XPS experiments represent a quantitative and surface-sensitive analytical technique to verify the chemical composition of the samples to support membrane formation. The existence of elements on the surface of samples was assessed by specific binding energy (eV) on XPS spectrum. In order to prevent excess contamination by carbon, oxygen and nitrogen species, the gold surface has been carefully precleaned with fresh hot Piranha solution prior to incubation in deaerated solutions containing compounds **Q_1S**, **Q_5S**, and **Q_{10}S**. The high-resolution XPS spectra then permitted direct quantification of the chemical species to provide detailed information for the composition on the gold surface. The data were processed by specific XPS software.

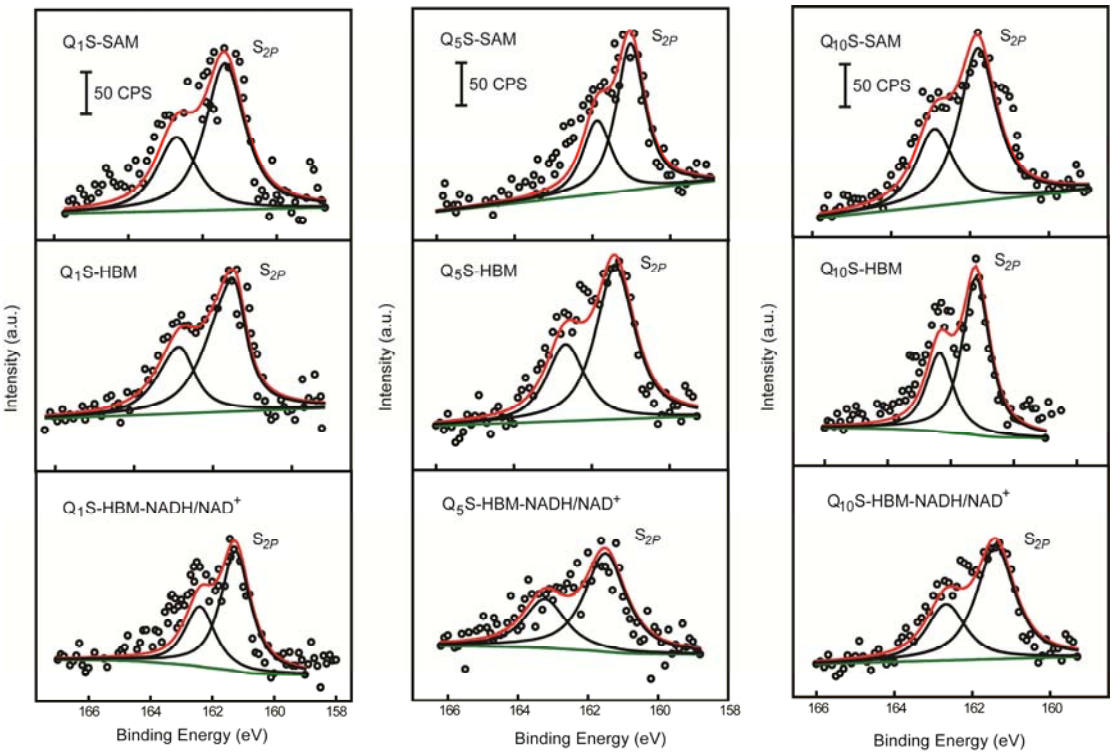

Figure S23-1. High-resolution XPS spectra of S_{2P} for **Q_nS**-SAMs, **Q_nS**-HBMs, and **Q_nS**-HBM-NADH/NAD^+. Open circles represent experimental raw data, red solid lines are for the total fits, black lines are for the component-fitted peaks, and green lines are for the baselines.

As shown in Figure S23-1, the XPS peaks of S_{2p} for **Q_nS**-SAMs, **Q_nS**-HBMs, and **Q_nS**-HBM-NADH/NAD^+ were fitted and deconvoluted to give the chemical shift data of the components within the coated molecules, respectively. Two dominant peaks located at ~161.5 and ~162.9 eV with an area ratio of 2:1 and a peak separation of ~1.2 eV were observed in the S_{2p} spectra, which could be assigned to the S atom bound on the gold surface.[15]

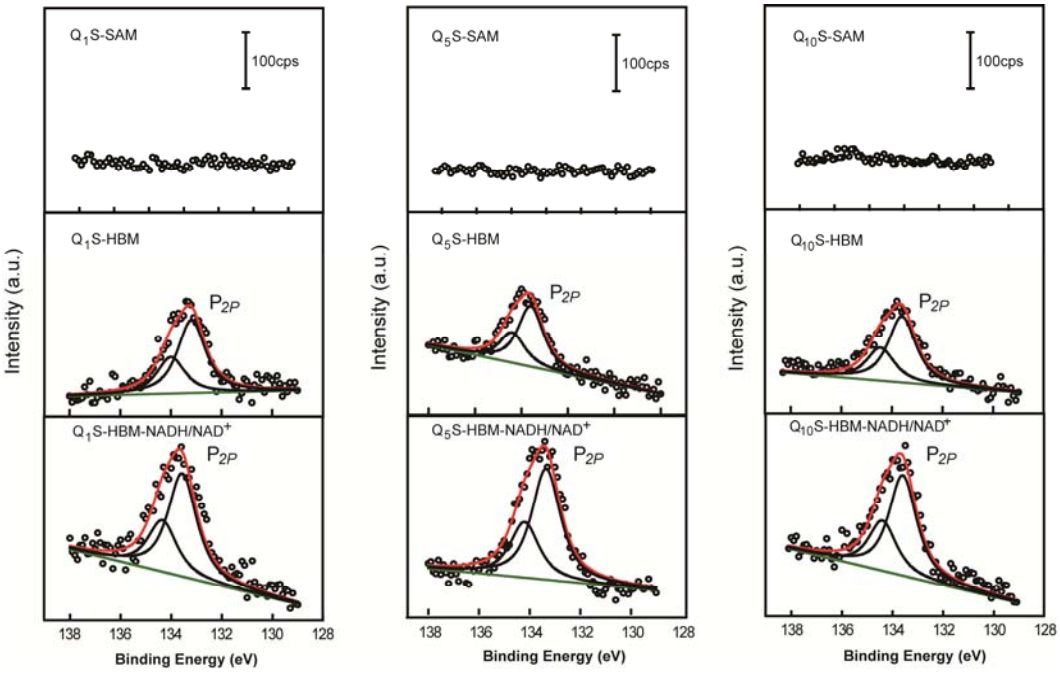

Figure S23-2. High-resolution XPS spectra of P_{2P} for **Q_nS**-SAMs, **Q_nS**-HBMs, and **Q_nS**-HBM-NADH/NAD^+. Open circles represent experimental raw data, red solid lines are for the total fits, black lines are for the component-fitted peaks, and green lines are for the baselines.

For proving the successful surface coating of lipids on **Q_nS**-SAMs, phosphorous was specifically scanned in that phosphorous only exists in lipid molecules. From Figure S23-2, the distinct peak of signals from 2p orbital of phosphorous correspond to P_{2p} at ~134.3 eV and ~133.6eV with an area ratio of 1:2 and a peak separation of ~1.3 eV.[16] These peaks qualitatively verify that lipid molecules form bilayers on **Q_nS**-SAMs since only lipid molecules consist of phosphorous.[17,18] Meanwhile, for **Q_nS**-HBM-NADH/NAD^+ system, we found the area of the phosphorous become larger than **Q_nS**-HBMs. Therefore, it can be confirmed that lipid membrane contained embedded NADH/NAD^+ following the established procedures of Fainstein and Bourdillon.

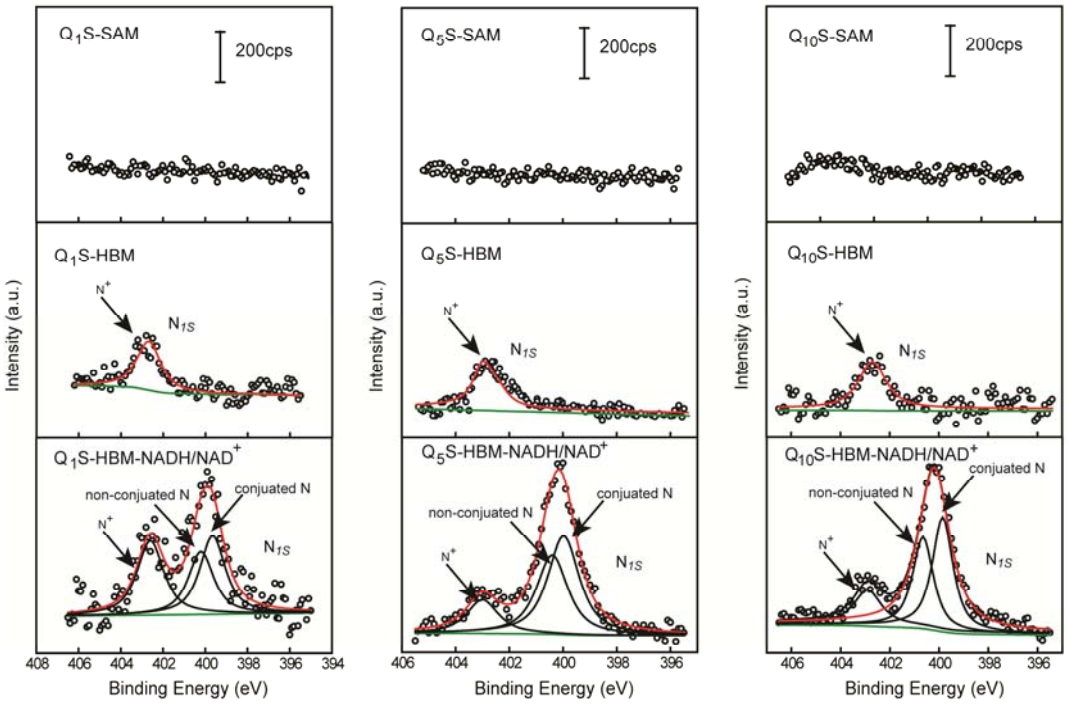

Figure S23-3. High-resolution XPS spectra of N_{1s} for **Q_nS**-SAMs, **Q_nS**-HBMs, and **Q_nS**-HBM-NADH/NAD^+. Open circles represent experimental raw data, red solid lines are for the total fits, black lines are for the component-fitted peaks, and green lines are for the baselines. The data of N_{1s} are fit with three components: the quaternary ammonium from lipid of egg PC (N^+, ~402.5 eV), the non-conjugated nitrogen (~400.6 eV) and the conjugated nitrogen (~399.0 eV) from NADH/NAD^+.

XPS confirmed the incorporation of lipid anchors at the gold surface. **Q_nS**-SAMs in Figure S23-3 show a XPS scan (from 410 to 390 eV region) that did not contain the lipid bilayer. The XPS spectrum did not reveal any spectra of N_{1s}. In contrast, the XPS of **Q_nS**-HBMs in Figure S23-3 showed a peak at binding energy about 402.5 eV, attributable to the quaternary ammonium (N^+) from lipid of egg PC.[19] The unique nitrogen composition for **Q_nS**-HBM-NADH/NAD^+ is observed in the nitrogen spectral differences from **Q_nS**-HBM in Figure S23-3. In the treatment of our data, we assign the high energy (~402.5 eV) peak to the quaternary ammonium (N^+) from lipid of egg PC; the low energy peak (400.6 eV) nonconjugated $-\overset{|}{\underset{}{N}}-$, –NH– and $–NH_2$ nitrogen and the lower energy peak (399.0 eV) to conjugated –N= from NADH/NAD^+.[20] They all have a peak separation of ~1.6 eV. The observed position of

the high resolution N_{1s} peaks in our samples is in good agreement with our proposed structure.

S5. Tapping-mode atomic force microscopy (TM-AFM)

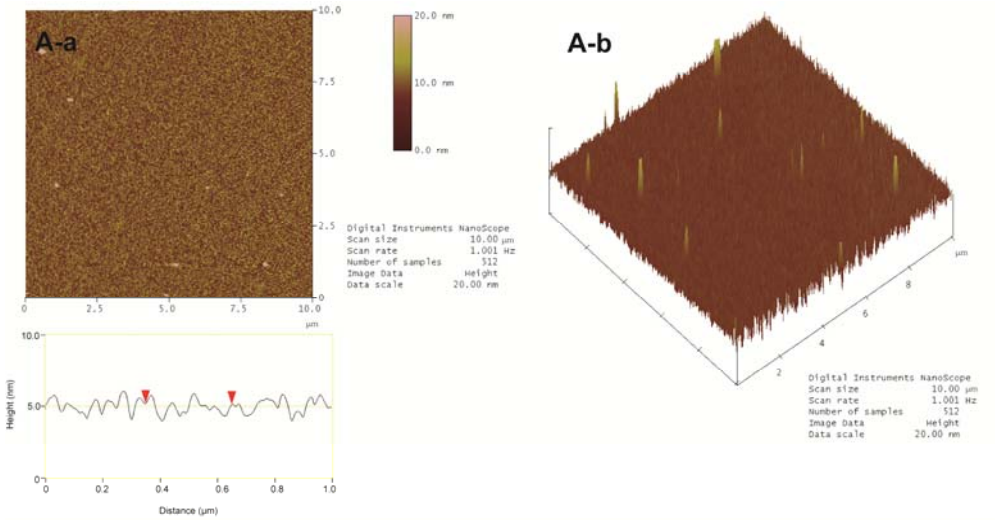

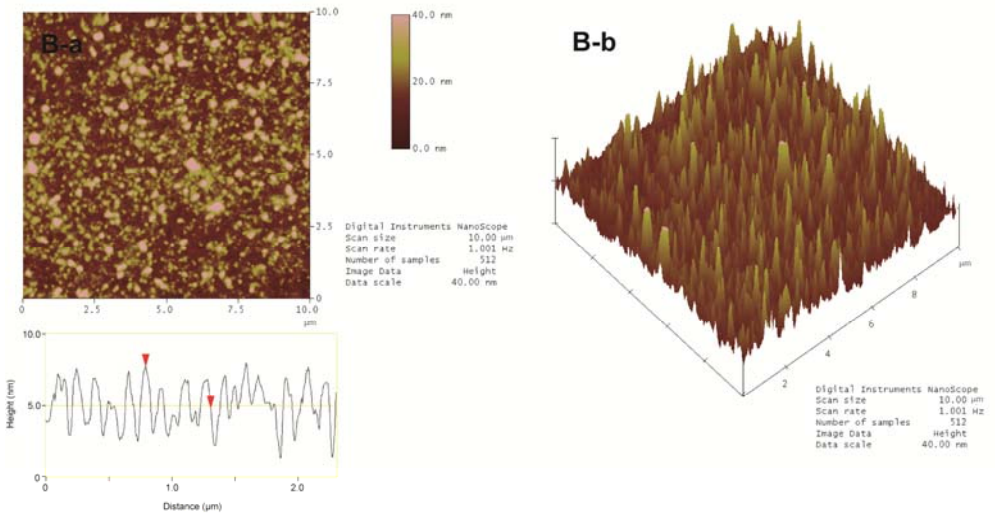

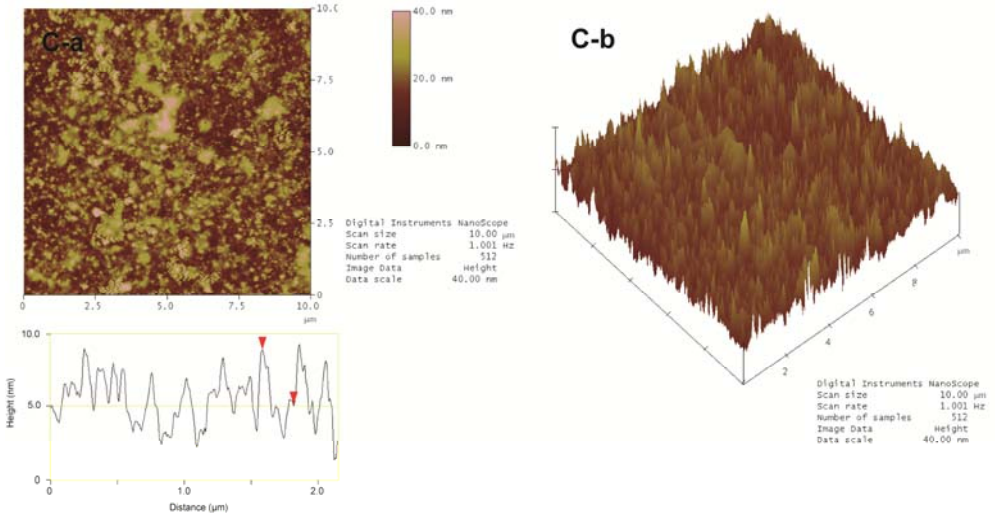

Figure S24. The AFM images showed the significant changes in the microscopic features on the electrode surface of (A):**Q_5S**-SAM; (B):**Q_5S**-HBM; and (C):**Q_5S**-HBM-NADH/NAD^+.

Figure S24 presents the topograph (a) and 3-D images (b) of the surfaces of **Q_5S**-SAM, **Q_5S**-HBM, and **Q_5S**-HBM-NADH/NAD^+. AFM measurements were carried out in tapping-mode on ubiquinone functionalized samples using the same protocol as that used for capacitance and XPS measurements.

Figure S24A shows the surface morphology of **Q_5S**-SAM electrode, as a mostly flat surface. The apparent depth of the **Q_5S**-SAM nanopatterns estimated from the cross section is consistent with the thickness of the alkylthiol-SAM (2.2-2.6 nm).[21] Figure S24B shows the surface topography of **Q_5S**-HBM on the gold surface, which is significantly different from the topography and 3-D images in Figure S24A. A large number of heightened areas are observed. Most of these are 5 ± 1 nm in height,[22] indicating the formation of a hybrid lipid bilayer was accomplished and it changed the topography of the gold surface. When NADH/NAD^+ is present in lipid bilayer, the topograph (a) and 3-D images (b) in Figure S24C is similar with Figure S24B. It is clear that the inclusion of NADH/NAD^+ has almost no effect on the double layer of the hybrid membrane. This indicates that NADH/NAD^+ does not induce large defects in the hybrid bilayer membrane.

S6. The kinetic analysis of Q_nS-HBMs using Laviron's formalism

The electrochemical behaviors of the **Q_nS**-HBMs on gold electrode were studied to investigate the effect of the scan rate on the heterogeneous electron-transfer kinetics. A series of well-defined redox peaks were observed and correspond to the electron-transfer process of the immobilized quinoid moiety at different scan rates for **Q_1S**-HBM, **Q_5S**-HBM and **Q_{10}S**-HBM in 0.1 M PBS of pH=7.4. The peak shapes are independent of scan rate. As shown in Figure S25A, C, E, the inspection of the curves revealed that an increase in the scan rates increases the current magnitude of both the anodic and cathodic peaks, which is expected assuming that the three ubiquinones undergo the quasi-reversible electron transfer reaction. For all tested **Q_nS**-HBMs both

the anodic and cathodic peak currents were found to be linearly proportional to scan rate from 20 to 180 $mV \cdot s^{-1}$, which is consistent with the voltammetric behavior of the surface confined redox center. Peak potentials shifted with increasing scan rate and peak separation increased, which is characteristic of an adsorbed redox species under kinetic control.

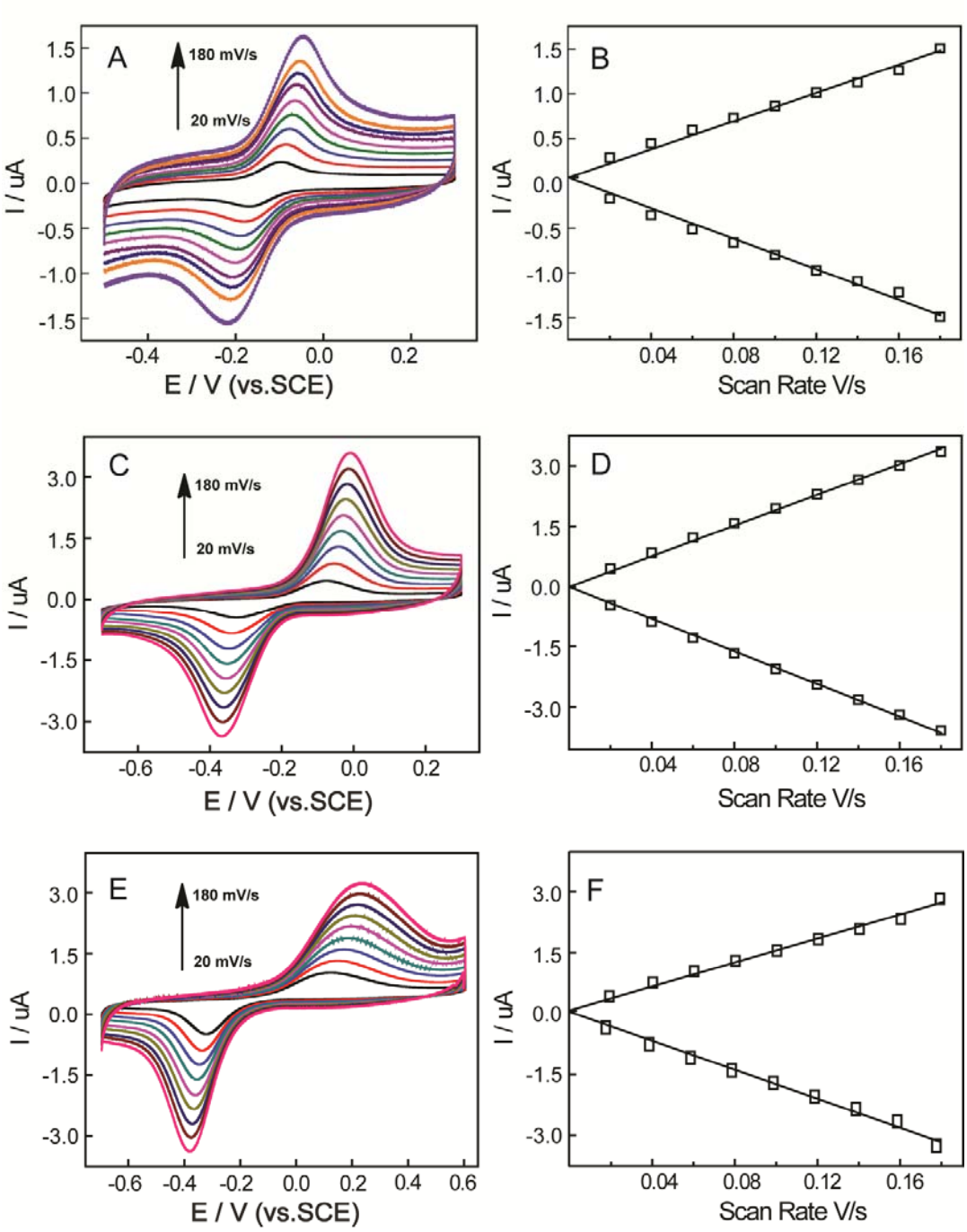

Figure S25. Cyclic voltammetric curves of $\mathbf{Q_nS}$-HBMs on gold electrodes (A) $\mathbf{Q_1S}$-HBM; (C) $\mathbf{Q_5S}$-HBM; (E) $\mathbf{Q_{10}S}$-HBM at the following scan rates: 20, 40, 60, 80,

100, 120, 140, 160, 180 $mV \cdot s^{-1}$ in 0.1 M PBS of pH=7.4 at 25 °C. Plots of **Q_nS**-HBMs anodic and cathodic peak currents on gold electrodes (B) **Q_1S**-HBM; (D) **Q_5S**-HBM; (F) **Q_{10}S**-HBM increase linearly with the scan rate.

To calculate the surface coverage (Γ,$mol \cdot cm^{-2}$) for **Q_nS**-HBMs, we used Equation 1 and integrated both cathodic and anodic peaks in the CVs to obtain Q. In Equation 1, n = the number of electrons exchanged per reactant molecule (considering the two-electron process for the ubiquinone/ubiquinol couple, n = 2), A = the area of the electrode and F is the Faraday constant.

$$\Gamma = Q/nFA \qquad 1$$

The geometric area of the gold electrode was used for the surface coverage calculation, and the surface roughness was assumed to be constant from the reproducible pretreatment of the gold electrodes. With these considerations, the surface coverage (Γ) was approximately 1.22×10^{-10} $mol \cdot cm^{-2}$ for **Q_1S**-HBM, 4.21×10^{-10} $mol \cdot cm^{-2}$ for **Q_5S**-HBM and 4.42×10^{-10} $mol \cdot cm^{-2}$ for **Q_{10}S**-HBM. While the coverage values of **Q_5S**-HBM and **Q_{10}S**-HBM is consistent with the typical surface coverage (Γ= $3.2 \sim 5.7 \times 10^{-10}$ $mol \cdot cm^{-2}$) found for the hydroquinone/quinone redox couple with alkyl spacers, **Q_1S**-HBM correspond to submonolayer coverage, suggesting that the only one methylene bridge does not pack tightly.

The Laviron approach, which is most commonly used obtaining heterogeneous rate constants ($k_{s,app}$) for electron transfer in redox-active SAMs was employed to evaluate the electron transfer rate. In this method, the peak separation is measured as a function of scan rate. Kinetic parameters, such as the standard rate constant (k_s) and the electron-transfer coefficient (α), may be obtained from equations 2 and 3[S23]

$$E_{pc} = E_c^{0'} - \frac{RT}{\alpha nF} \ln\left(\frac{\alpha nF \upsilon_c}{RTk_{app}}\right) \qquad (2)$$

$$E_{pa} = E_a^{0'} - \frac{RT}{(1-\alpha)nF} \ln\left(\frac{(1-\alpha)nF \upsilon_a}{RTk_{app}}\right) \qquad (3)$$

where E_{pc} and E_{pa} are the potentials of the cathodic and anodic peaks, the peak potential separation $| E_{pa} - E_{pc} |$ is larger than 200mV/n, n is the number of electrons transferred, and υ_a and υ_c are the critical scan rates. These last two parameters are

obtained for both the anodic and the cathodic branches by plotting E_p versus ln(υ) and extrapolating the linear portion back to the x-axis intercept, giving the formal potentials $E^{0'}_{pa}$ and $E^{0'}_{pc}$, $E^{0'}_{pa}$ is equal to $E^{0'}_{pc}$. The slope of these lines provides the transfer coefficients values that can be used to determine the apparent heterogeneous rate constants. Ideally, the rate constants and transfer coefficients obtained from the two branches of the CVs are self-consistent. The slopes of the linear portion of the E_p versus ln(ν) curves are RT/nαF for the cathodic branch and RT/n(1-α)F for the anodic branch. The values of nα and n(1-α) were obtained from the values of each slope and substituted back in equations 2 and 3 to solve for k_{app}. The two apparent rate constants (k_{app}) obtained in this way were averaged, and their average value was denoted by k_{app}, shown in Table 1. The value is in accordance with that obtained from the equations 6, where the intercepts (I) and slopes (S) for the linear portion of the E_p versus ln(ν) curves are directly linked with k_{app}.

$$k_{app,c} = \frac{\alpha n F \upsilon_c}{RT} \quad (4)$$

$$k_{app,a} = \frac{(1-\alpha) n F \upsilon_a}{RT} \quad (5)$$

$$(S_a + S_c) \ln \kappa_{app} = I_c - I_a - S_a \ln S_a - S_c \ln S_c \quad (6)$$

Table S1. Electrochemical Kinetic Parameters of **Q_nS**-HBMs (n=1, 5, 10) on a Au Electrode[a]

Spacer length	αn	(1-α)n	$\log(k_{app})/s^{-1}$
1	1.08	1.16	-0.67
5	1.46	0.74	-2.28
10	1.78	0.36	-4.59

[a] The values of nα and n(1-α) are transfer coefficients due to reduction and oxidation of ubiquinone for overall reaction under the assumption that n = 2. The value of k_{app} is the average value of anodic and cathodic apparent rate constants for overall redox reaction.

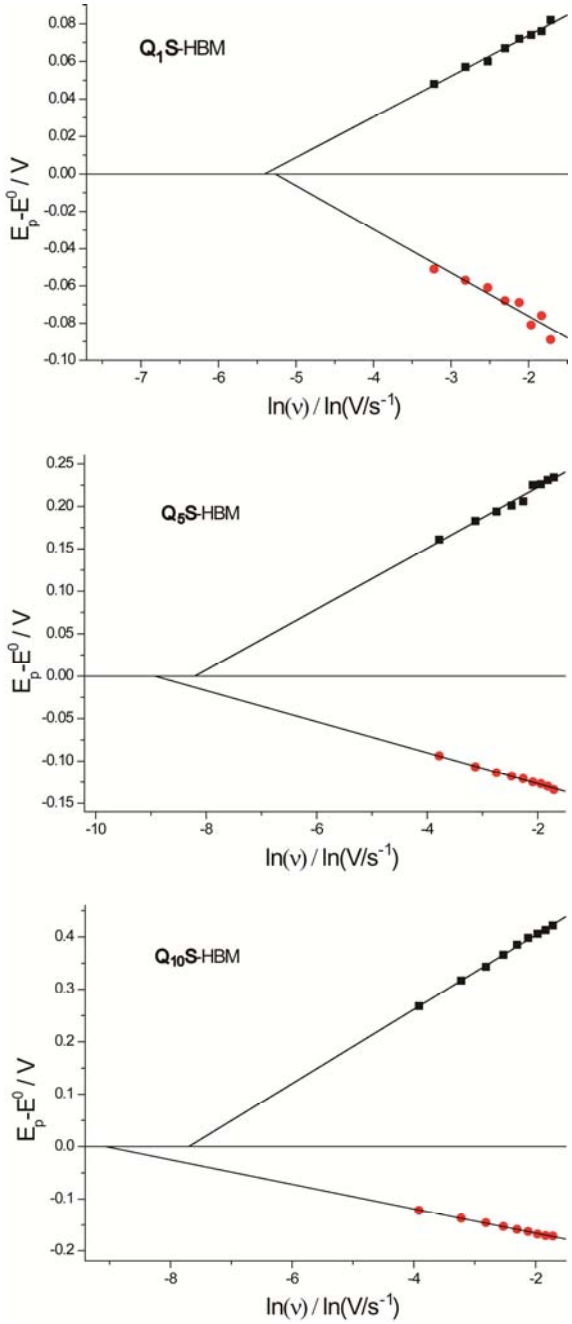

Figure S26. Charge-transfer rate analysis of **Q_nS**-HBMs using the Laviron formalism.

Figure S26 shows the plot of E_{pa} and E_{pc} versus the natural logarithm of the scan rate. A linear best fit to data points that meet the peak separation criterion leads to determination of the charge-transfer coefficient (α) and the apparent rate constant of charge transfer (k_{app}) by the intercept of the fit line with $E_p - E_0 = 0$, termed the critical scan rate. The Laviron formalism gives α values approaching 0.5 and apparent charge transfer rates, *k*app, of 0.21, 0.005, and 0.006s^{-1} for **Q_1S**-HBM, **Q_5S**-HBM and **Q_{10}S**-HBM, respectively.

S7. Control experiments

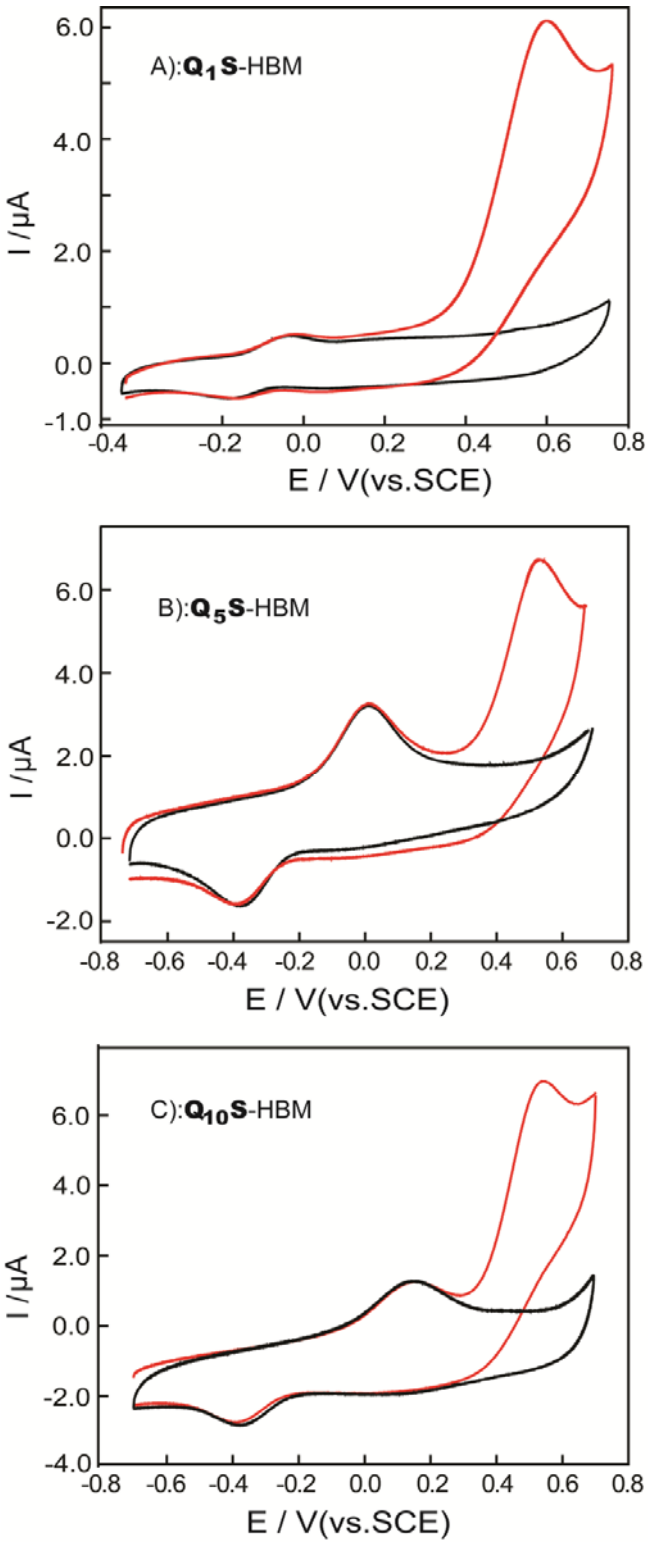

Figure S27. Voltammetric responses of ubiquinone-embedded HBM systems (**Q_nS**-HBM) that does not contain NADH/NAD+ in the lipid membrane, and instead NADH/NAD+ was added to the PBS buffer (pH 7.4) under nitrogen atmosphere.

(A):**Q_1S**-embedded HBM systems; (**Q_1S**-HBM) (B):**Q_5S**-embedded HBM systems (**Q_5S**-HBM); (C):**Q_{10}S**-embedded HBM systems (**Q_{10}S**-HBM), respectively.

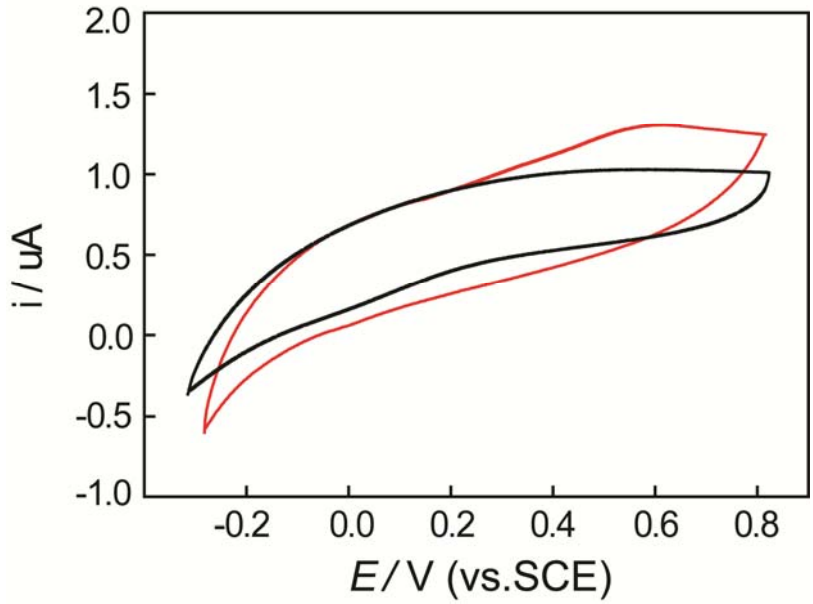

Figure S28. Voltammetric responses of the hexanethiol-embedded HBM system in the absence (a) and presence (b) NADH/NAD^+ in lipid bilayer membrane in 0.1M PBS of pH 7.0 under nitrogen atmosphere.

In order to compare the redox potential values in our biomimetic membrane model with the reported formal potentials of ubiquinone and NADH in reference, a detailed discussion is now provided.

The formal potential values of surface-confined **Q_nS** (**Q_1S**:-0.11 V vs SCE, **Q_5S**:-0.10 V vs SCE and **Q_{10}S**:-0.08 V vs SCE) as assessed by cyclic voltammetry are in agreement with the reported value of ubiquinone at -0.13 V *vs* SCE of pH 7.0 (Table S2, Supporting Information).[S24,S25] The reversible redox potential for NADH/NAD^+ is reported as -0.56 V vs SCE at pH 7.0 (Table S2, Supporting Information) [S26,S27] and the direct oxidation of NADH at bare electrodes, in general, requires high overpotential that can be as large as 1.0 V. In our biomimetic membrane model, this high overpotential is substantially decreased and reversible interconversion between NADH and NAD^+ could be achieved when both surface-modified ubiquinone as a redox mediator and NADH/NAD^+ are immobilized in the lipid membrane.

Table S2. Anodic peak potentials (E_a/V), cathodic peak potentials (E_c/V) and formal potential (E_f/V) of **Q_nS**-HBM-NADH/NAD^+ in the biomimetic membrane model. In addition, the reported formal potential values of ubiquinone and NADH in lipid membranes are included.

	ubiquinone			NADH/NAD^+		
	E_a/V[a]	E_c/V[b]	E_f/V[c]	E_a/V[a]	E_c/V[b]	E_f/V[c]
Q_1S-HBM-NADH/NAD^+	-0.04	-0.18	-0.11	0.16	0.08	0.12
Q_5S-HBM-NADH/NAD^+	0.10	-0.30	-0.10	0.38	0.22	0.30
Q_{10}S-HBM-NADH/NAD^+	0.17	-0.32	-0.08	0.50	0.20	0.35
Literature Values			-0.13			-0.56

[a] Anodic peak potential *vs* SCE at scan rate of 100 mV·s^{-1} in 0.1M phosphate buffer solution of pH 7.0. [b] Cathodic peak potential *vs* SCE at scan rate of 100 mV·s^{-1} in 0.1M phosphate buffer solution of pH 7.0.[c] Formal redox potential *vs* SCE at scan rate of 100 mV·s^{-1} in 0.1M phosphate buffer solution of pH 7.0.

S8. Spectroelectrochemical UV-vis experiments (enzymatic assay)

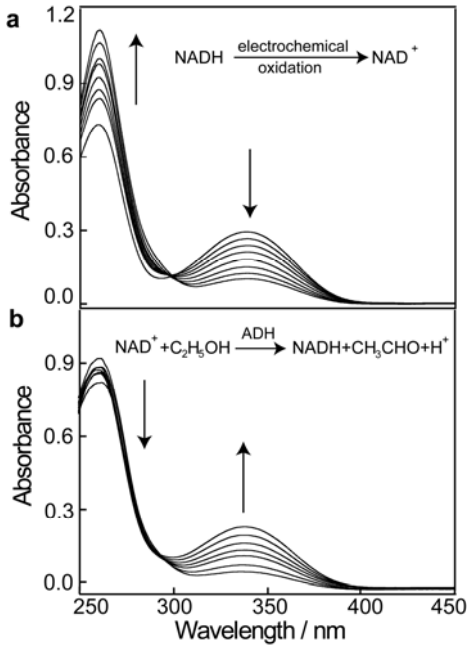

Figure S29. **a**) The disappearance of NADH monitored by UV–vis (peak at 340 nm) using a **Q_5S**-HBM on gold mesh electrode at applied potential of ~0.50 V vs

Ag/AgCl with incident 473 nm laser. **b**) The enzymatic consumption (alcohol dehydrogenase, ethanol) of NADH monitored by UV–vis (peak at 340 nm).

S9. References

(S1) Han, X. J.; Critchley, K.; Zhang, L. X.; Pradeep, S. N. D.; Bushby, R. J.; Evans, S. D. *Langmuir* **2007**, 23, 1354-1358.

(S2) Daza Millone, M. A.; Vela, M. E.; Salvarezza, R. C.; CreczynskiPasa, T. B.; Tognalli N. G.; Fainstein, A. *ChemPhysChem* **2009**, 10, 1927-1933.

(S3) Marchal, D.; Pantigny, J.; Laval, J. M.; Moiroux, J.; Bourdillon, C. *Biochemistry* **2001**, 40, 1248-1256.

(S4) Jeuken, L. J. C.; Connell, S. D.; Henderson, P. J. F.; Gennis, R. B.; Evans, S. D.; Bushby, R. J. *J. Am. Chem. Soc.* **2006**, 128, 1711-1716.

(S5) Plant, A. L. *Langmuir* **1999**, 15, 5128-5135.

(S6) Long, Y. T.; Sutherland, T. C.; Kraatz, H. B.; Lee, J. S. *Chem. Commun.* **2004**, 2032-2033.

(S7) Carpino, L. A.; Triolo, S. A.; Berglund, R. A. *J. Org. Chem.* **1989**, 54, 3303-3310.

(S8) Lipshutz, B. H.; Bülow, G.; Lowe, R. F.; Stevens, K. L. *Tetrahedron* **1996**, 52, 7265-7276.

(S9) Ohkawa, S.; Terao, S.; Terashit , Z.; Shibouta, Y.; Nishikawa, K. *J. Med. Chem.* **1991**, 34, 267-276.

(S10) Laura, P. P.; Sarah, G. K.; Mark, V. W.; Ronald, B.; Kumar, S. *Langmuir* **2008**, 24, 11556–11561.

(S11) Alison, M. D.; Andrew, D. A. *Org. Biomol. Chem.* **2004**, 2, 2371-2375.

(S12) Hong, H. G.; Wonchoul, P. *Langmuir* **2001**, 17, 2485-2492.

(S13) Milalsayuki, K.; Yasutaka, A.; Shiho, O.; Takuya, N.; Akihiko, H.; Yoshiro, H. *Synthesis* **2007**, 21, 3286–3289.

(S14) Kelso, G. F.; Porteous, C. M.; Coulter, C. V.; Hughes, G.; Porteous, W. K.; Ledgerwood, E. C.; Smith, R. A. J.; Murphy, M. P. *J. biol. Chem.* **2001**, 276, 4588-4596.

(S15) Ishida, T.; Yamamoto, S.; Mizutani, W.; Motomatsu, M.; Tokumoto, H.; Hokari, H.; Azehara, H.; Fujihira, M. *Langmuir* **1997**, 13, 3261-3265.

(S16) Ignatova, M.; Manolova, N.; Lachkova, V.; Varbanov, S.; Rashkov, I. *Macromol. Rapid Commun.* **2008**, 29, 1871-1876.

(S17) Liu, Y. T.; Li, K.; Pan, J.; Liu , B.; Feng ,S. S. *Biomaterials* **2010**, 31, 330-338.

(S18) Rouxhet, P. G.; Misselyn-Bauduin, A. M.; Ahimou, F.; Genet, M. J.; Adriaensen, Y. ; Desille, T.; Bodson, P.; Deroanne, C. *Surf. Interface Anal.* **2008**, 40, 718-724.

(S19) Yao, C.; Li, X. S.; Neohb, K. G.; Shi, Z. l.; Kang' E. T. *J. Membr. Sci.* **2008**, 320, 259-267.

(S20) Saprigin, A. V.; Thomas, C. W.; Dulcey, C. S.; Patterson Jr, C. H.; Spector, M. S. *Surf. Interface Anal.* ***2004***, 36, 24-32.

(S21) Bain, C. D.; Troughton, E. B.; Tao, Y. T.; Evall, J.; Ehitesides, G. M.; Nuzzo, R. G. *J. Am. Chem. Soc.* **1989**, 111, 321.

(S22) Tero, R.; Takizawa, M.; Li, Y. J.; Yamazaki, M.; Urisua, T. *Appl. Surf. Sci.* **2004**, 238, 218-222.

(S23) Laviron, E. J. *Electroanal. Chem.* **1979**, 101, 19-28.

(S24) Moncelli, M. R.; Herrero, R.; Becucci, L.; Guidelli, R. *Biochim. Biophys. Acta* **1998**, 1364, 373-384.

(S25) Elliott, S. J.; Léger, C.; Pershad, H. R.; et al. *Biochim. Biophys. Acta* **2002**, 1555, 54-59.

(S26) Pariente, F.; Tobalina, F.; Moreno, G.; et al. *Anal. Chem.* **1997**, 69, 4065-4075

(S27) Karyakin, A. A.; Ivanova,Y. N.; Karyakina, E. E. *Electrochem. Commun.* **2003**, 5, 677-680.